Agricultural Water Management 329 (2026) 110343

Contents lists available at ScienceDirect

Agricultural Water Management

journal homepage: www.elsevier.com/locate/agwat

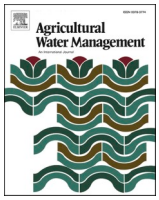

Climate warming accelerates maize phenology and reduces water requirements and yields in south-eastern Kazakhstan

Baktybek Duisebek [a,1], Maria Shahgedanova [a,*], Andrew J. Wade [a], Ragab Ragab [b], Zarina Saidaliyeva [a,c], Nikolay Kasatkin [c]

[a] Department of Geography and Environmental Science, University of Reading, Reading, UK
[b] UK Centre for Ecology and Hydrology (UKCEH), Wallingford, UK
[c] Central Asia Regional Glaciological Centre under the Auspices of United Nations Educational, Scientific and Cultural Organization (UNESCO), Almaty, Kazakhstan

ARTICLE INFO

Handling Editor Enrique Fernandez

Key words:
Crop-water modelling
AquaCrop
SALTMED
Irrigation
Climate change
Adaptation
Tien Shan
Central Asia

ABSTRACT

This study assesses the impacts of climate change on maize water requirements and yields in south-eastern Kazakhstan, a semi-arid region dependent on meltwater from the Tien Shan Mountains for irrigation. The region is experiencing significant warming, projected to continue, leading to cryosphere degradation and reduced meltwater availability. Using field data collected between 2016 and 2019, two crop–water models (AquaCrop and SALTMED) were calibrated and validated to simulate maize growth, water demand, and yield at a farm located in the Tien Shan foothills under future climate scenarios. Simulations were driven by downscaled and bias-corrected outputs from four Global Circulation Models under Representative Concentration Pathways (RCP) 4.5 and 8.5 for 2020–2049, 2040–2069, and 2070–2099. Results show that continued warming will shorten the maize growing season by 36–38 days (RCP4.5) and 42–45 days (RCP8.5), reducing crop water requirements by 11–15% (AquaCrop) and 16–24% (SALTMED) by 2100 relative to the 1976–2005 baseline. AquaCrop projects a 10–12% yield reduction by 2100, with statistically significant declines by mid-century under both scenarios. SALTMED projects a 7–8% reduction by 2100, with significance emerging in the late century under RCP4.5 and mid-century under RCP8.5. These changes are primarily driven by temperatures exceeding maize's physiological optimum. The findings align with global evidence of accelerated phenology and reduced maize productivity under climate warming. Adopting efficient irrigation systems, adjusting sowing dates, and selecting shorter-maturing cultivars could help align water demand with peak rainfall and runoff, sustaining yields under declining meltwater availability.

1. Introduction

Climate change is affecting global food security through rising temperatures, shifting precipitation patterns, and more frequent extreme weather events (Mbow et al., 2019), with substantial changes in global crop yields projected as early as the 2040 s (Jägermeyr et al., 2021). In low-latitude regions (0–30°), crop yields are expected to decline. Impacts in mid-latitude regions (30–60°) are less certain, with the direction and magnitude of change depending on crop type, geographic location and agricultural practices, particularly the extent of irrigation use (Challinor et al., 2014; Ray et al., 2015; 2019; Liu et al., 2016).

Central Asia (CA) is a mid-latitude region characterized by extensive plains dominated by arid and semi-arid environments and bordered by the glacierized Tien Shan and Pamir mountains, where elevations reach up to 7,000 m a.s.l. The region comprises five developing countries with growing populations, where agriculture makes a significant contribution to national GDP and accounts for approximately 35% of regional employment (Saidaliyeva et al., 2024). Observed temperature increases in CA exceeded the global average during the 1881–2016 period (Groisman et al., 2017; Yao et al., 2022), while future projections estimate a warming of 2–6°C by the end of the century, depending on the scenario and model used (Fallah et al., 2024). These trends, combined with the region's strong dependence on meltwater from the mountain cryosphere, position CA as a climate-change impact hotspot (Groisman

* Corresponding author.
E-mail address: m.shahgedanova@reading.ac.uk (M. Shahgedanova).
[1] Permanent address: School of IT and Engineering, Kazakh-British Technical University, Almaty, Kazakhstan; Department of Water Resources and Melioration, Kazakh National Agrarian Research University, Almaty, Kazakhstan.

https://doi.org/10.1016/j.agwat.2026.110343
Received 3 November 2025; Received in revised form 12 March 2026; Accepted 8 April 2026
Available online 11 April 2026

et al., 2017; Vakulchuk et al., 2022).

Meltwater from mountain snowpack and glaciers contributes approximately 70 – 80% of total runoff in the region and therefore serves as a critical source of irrigation water (Viviroli and Weingartner, 2004; Murzakulova et al., 2019; Saidaliyeva et al., 2024). Extensive glacier shrinkage has been observed in the Tien Shan since the mid-20th century (Pieczonka, Bolch, 2015; Farinotti et al., 2015) and is projected to continue (Hock et al., 2019; Shannon et al., 2019). Peak flow is expected to pass by the 2040s–2050 s in the outer ranges of the Tien Shan (Hock et al., 2019; Shahgedanova et al., 2020), putting water provision at risk.

Kazakhstan, the largest country in CA, is among the world's leading grain producers. Its extensive rain-fed wheat cultivation is concentrated in the northern regions and plays a crucial role in national food security and global grain exports (Schmitz and Meyers, 2015). The impacts of climate change on large-scale cereal production in northern Kazakhstan have been investigated (Lioubimtseva and Henebry, 2009; Fay et al., 2010; Mirzabaev, 2013; Sommer et al., 2013; Bobojonov and Aw-Hassan, 2014; Eisfelder et al., 2014; Morgounov et al., 2014; Pavlova et al., 2014; Reyer et al., 2017). In contrast, climate change impacts on arable agriculture in south-eastern Kazakhstan (SEK) have received little attention. In SEK, small (< 30 ha) and medium (30 – 90 ha) scale family and tenant farms dominate in the foothills of the glacierized Tien Shan mountains (Barrett et al., 2017). A variety of crops such as maize, soy, wheat, alfalfa, potatoes and various vegetables, are primarily grown on irrigated land, with produce marketed both regionally and across national borders. These farms contribute significantly to the regional economy but are particularly vulnerable to climate change due to low adaptive capacity. This vulnerability arises from limited financial resources, restricted access to technical expertise, and dependence on deteriorating irrigation infrastructure, which is often outside the farmers' control (Barrett et al., 2017; Murzakulova et al., 2019; FAO, 2025).

Crop water models provide an effective means for quantifying the impact of climate and agricultural practices on crop water use and yields (Keulen, 2013). Combined with observational climatic records and future climate projections, they can inform adaptation strategies that increase resilience to climate change (Harvey et al., 2018). However, crop models have not been widely applied in SEK and their use across CA has been limited (e.g., Kato et al., 2012; Akhtar et al., 2013; Sommer et al., 2013; Pavlova et al., 2014; Nizamov et al., 2023; Sherzod et al., 2023) apart from global crop model intercomparison projects (e.g., Jägermeyr et al., 2021) largely due to a scarcity of climate, soil, and yield data.

Maize is a widely grown crop in SEK. It is a food staple or used as animal fodder. Rising temperatures and potential water shortages pose significant risks to maize productivity. In particular, maize pollen viability declines with prolonged exposure to temperatures above 32°C and even short exposure to temperatures above 38°C (Herrero and Johnson, 1980). Heat stress during critical stages such as anthesis and early grain filling can result in grain sterility, abortion, and accelerated senescence (Crafts-Brandner and Salvucci, 2002). A threshold of 35°C is often used as an indicator of suboptimal conditions for maize growth (Hatfield and Prueger, 2015), and studies in north-eastern China have shown that projected yield declines were primarily driven by temperatures exceeding this threshold (Guo et al., 2017; Jiang et al., 2021). The negative effects of heat are amplified under conditions of high vapour pressure deficit (VPD), as pollen viability prior to silk reception is closely linked to pollen moisture content, which in turn is strongly influenced by VPD (Fonseca and Westgate, 2005). Maize's sensitivity to heat extremes is further exacerbated by its short flowering period of only 3–5 days, meaning that a single extreme heat event can compromise all pollinating flowers (Hatfield and Prueger, 2015). Elevated night-time temperatures influence plant respiration rates, potentially reducing biomass accumulation and overall yield (Hatfield et al., 2011). Frost can also damage seedlings and cause establishment failure, and a reduction in frost days may provide some benefit (Dhillon et al., 1988).

Drought damages maize crops particularly if they occur during the flowering and grain-filling stages, with potential yield losses ranging from 40% to 90% (Çakir, 2004). Using satellite and field data, Lobell et al. (2011) showed that global maize yields declined by 5.5% due to temperature increases observed since the 1980s. Similarly, Lobell et al. (2014) found that the 2012 USA Midwest drought caused substantial yield losses, particularly among modern high-yielding maize varieties, which are more sensitive to drought stress.

This study aims to quantify the impacts of the observed climatic variability and future climate change on water requirements and yields of irrigated maize in SEK at farm scale. Specifically, it:

(i) Simulates maize yields and crop water requirement (CWR) using AquaCrop and SALTMED crop–water models calibrated with the newly obtained, extensive climate, soil, and crop data;
(ii) Applies downscaled and bias-corrected climate projections from four General Circulation Models (GCM) under two Representative Concentration Pathways: RCP4.5 (moderate) and RCP8.5 (high);
(iii) Assesses the impacts of future climate change on maize phenology, water requirements, and yields, and their implications for crop and irrigation management and adaptation.

As a C4 crop, maize has limited capacity to benefit from elevated atmospheric CO_2 (Kimball, 2016), so CO_2 fertilization effects are not considered in this study. While spring and summer phenological stages were well defined through field observations, autumn markers were less consistent due to variability in harvest timing, which is depended on the availability of combine harvesters and storage facilities. Therefore, the crop growth cycle (CGC) is defined here as the period between sowing and physiological maturity.

2. Materials and methods

2.1. Study area

The study was conducted in the foothills of the Ile Alatau range, part of the northern Tien Shan Mountains in south-eastern Kazakhstan (Fig. 1). A maize field (43.50 N, 76.95 E), located in the Karaoi district in the Ile Region of Almaty Oblast' (region) near Almaty, the largest city of Kazakhstan with population just under 2 million, was used as an experimental site (Fig. 1). The field (16 ha) is part of a private farm. Experimental data were collected between 2016 and 2019.

The study region has a continental climate classified as semi-arid grassland steppe according to the Köppen-Geiger classification (Beck et al., 2018). Air temperature and precipitation exhibit strong seasonal variability (Fig. 2). Mean monthly air temperatures range from -10°C in January to 25°C in July. Precipitation peaks in April–May and reaches minimum in August. Mean total precipitation during June–July–August (JJA) was 81 mm for the 1961–2019 period. Maize evapotranspiration (ETc), estimated using the FAO Penman–Monteith equation (Allen et al., 1998) with data from the Automatic Weather Station (AWS) (Fig. 1), was approximately 380 mm during JJA. This large gap between water demand and precipitation indicates that crop production in the region is highly dependent on irrigation.

River runoff, driven by snowmelt in May–June and glacier melt in July–August, peaks between May and August and provides essential irrigation water (Shahgedanova et al., 2018). In 2017, glaciers on the northern slope of the Ile Alatau covered a total area of 148 km^2, representing a 48% reduction in area since 1956 (Kokarev et al., 2023). The Tuyuksu Glacier, a World Glacier Monitoring Service (WGMS) benchmark glacier located within the study area, has shown a persistently negative cumulative mass balance, with an average loss of 0.40 m water equivalent per year over the 1958–2016 period (Kapitsa et al., 2020). These trends are projected to continue (Shannon et al., 2019; Shahgedanova et al., 2020).

Kastanozem soils are the dominant soil type in the region, followed

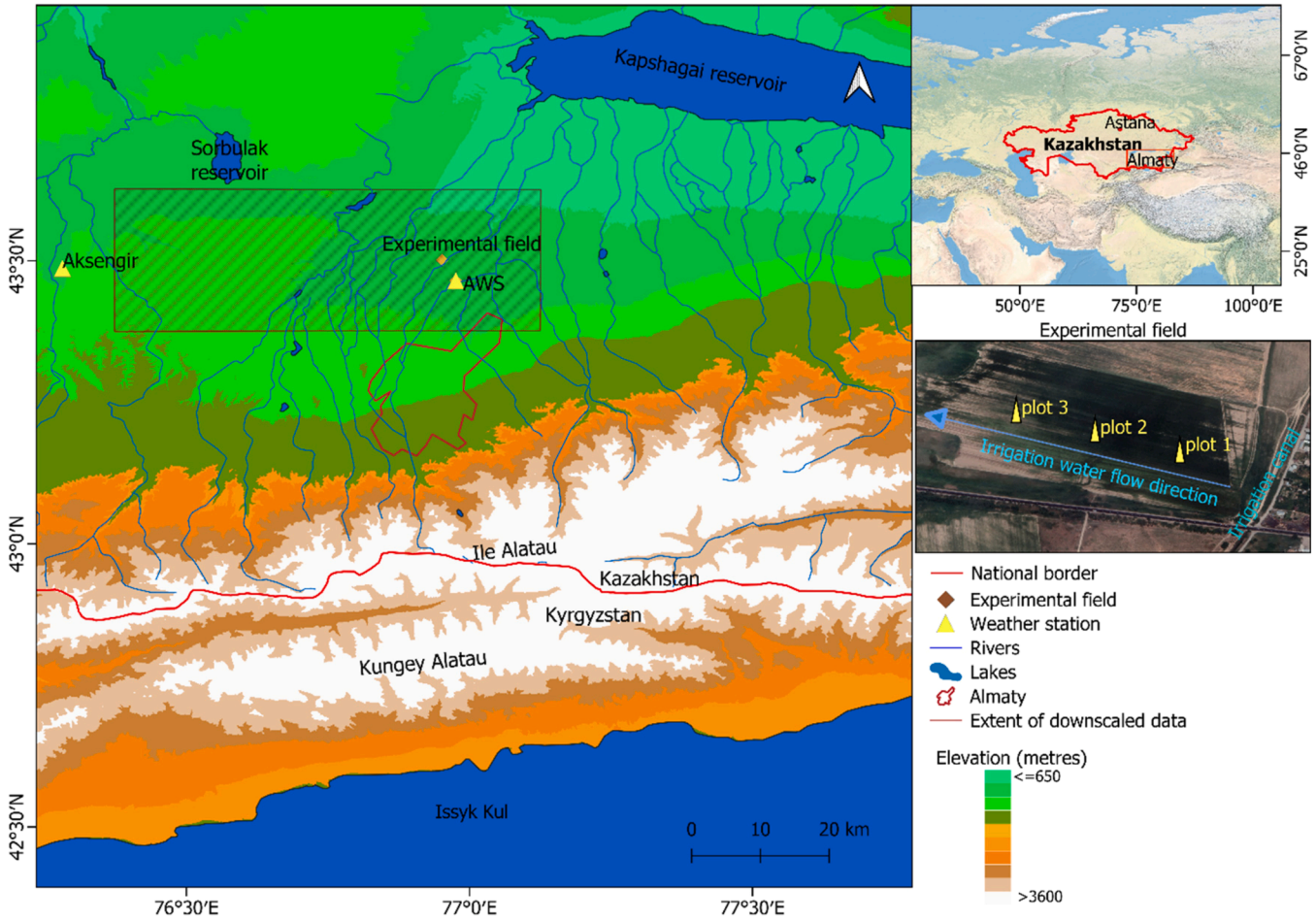

Fig. 1. Location of the study area, experimental field, and weather stations. The grey box indicates the area for which climate projections were downscaled. The background is a Digital Elevation Model (DEM) derived from Shuttle Radar Topography Mission (SRTM) data. National borders and water bodies are from ESRI ArcGIS Hub. The satellite image of the experimental field shows land cover in July 2019 (Google Earth).

by Calcisols, Cambisols, Chernozems, and Luvisols (Sokolov et al., 2017; Poggio et al., 2021). The irrigated agricultural zone lies between 400 and 800 m a.s.l., primarily on Kastanozem soils.

2.2. AquaCrop and SALTMED

AquaCrop (Raes et al., 2009; Steduto et al., 2009; Hsiao et al., 2009) and SALTMED (Ragab, 2002; 2015) models were used to quantify the maize CWR and yield. The data requirements of both models relate to climate, crop, soil and management (Table 1) and these were collected between 2016 and 2019.

CWR is the amount of water required to compensate for crop evapotranspiration (ETc) during plant growth and is equal to the reference crop evapotranspiration (ETo) multiplied by the crop coefficient (Kc) for maize. Both AquaCrop and SALTMED have been used extensively to simulate CWR and irrigation requirements for single or multiple growing seasons and with a wide variety of crop types under different climate conditions (FAO, 2017; Ragab, 2002). The Penman-Monteith equation (Allen et al., 1998) is embedded in both the AquaCrop and SALTMED models to estimate ETo using air temperature, relative humidity, wind speed and sunshine hours (or solar radiation) data. Both models are ideally suited for simulating CWR and yields when water is the key factor limiting crop growth.

In SALTMED, stage-specific Kc values corresponding to the initial, development, mid-season, and late-season growth phases were input directly, based on the Food and Agriculture Organisation (FAO) guidelines (Allen et al., 1998). The model interpolates these values to derive daily Kc values across the growing cycle from sowing to senescence. In contrast, AquaCrop internally calculated daily Kc values by applying a predefined maximum Kc and dynamically adjusting it according to crop development stages. Soil water retention was calculated by both models. For example, in SALTMED, the soil water content–water potential and the soil water potential–hydraulic conductivity relationships, required to solve the water and solute transport equations, were calculated using the Van Genuchten (1980) equation and a range of soil physical parameters (Ragab, 2015). The SALTMED model has a nitrogen dynamics component and crop nitrogen uptake is one of the processes represented. Nitrogen availability is considered in the biomass production process.

2.3. Observational and modelled climate data

2.3.1. Observational climate data

Meteorological data were obtained from the Aksengir station, operated by the Kazakhstan National Hydrometeorological Service, and from a Campbell Scientific AWS (Fig. 1). Aksengir, located approximately 50 km west of the site at similar elevation and land cover, provided daily records from 1961 to 2019. The AWS was installed at the experimental site of the Kazakh National University AgroBio Centre, approximately 3.5 km south-east of the experimental field, and provided hourly data on precipitation, air temperature, relative humidity (RH), wind speed, and the four components of radiation between 2016 and 2019. Due to missing AWS temperature data in 2016 and underestimation of winter precipitation from the unheated rain gauge, AquaCrop and SALTMED simulations used Aksengir data for temperature and precipitation, and

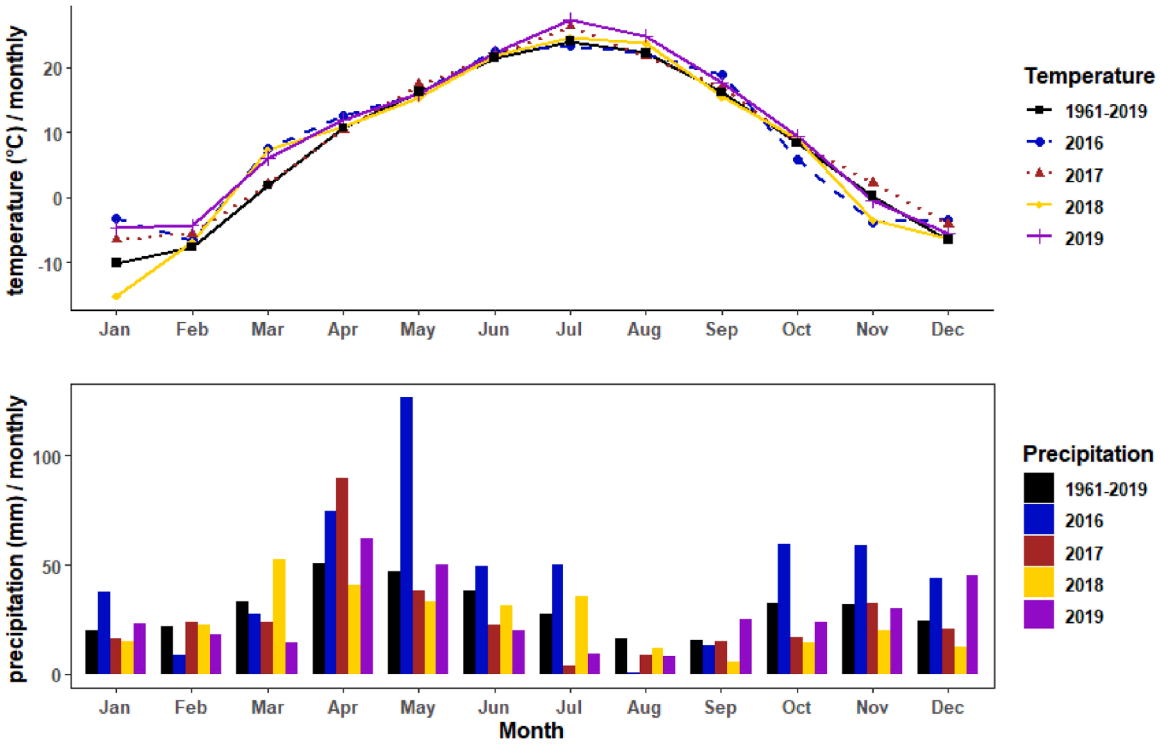

Fig. 2. Monthly temperature and precipitation at Aksengir meteorological station (Fig. 1) in 2016–2019 in comparison with the 1961–2019 mean monthly values.

Table 1
AquaCrop and SALTMED input data requirements.

Data type	Time series and constants required
Climate	Air temperature, incoming solar radiation, precipitation, wind speed, relative humidity
Crop	Crop type, crop growth stages, crop coefficients (k_c), root depth, plant density, plant height, and Leaf Area Index (LAI).
Soil	Soil texture, field capacity, wilting point, soil depth, bulk density, and Soil Water Content (SWC).
Management	Irrigation practices (method, quantity and salinity of water), fertilizer and pesticide application, tillage practices, crop rotation.

AWS data for RH, wind speed, and radiation to calculate reference evapotranspiration (ETo). The long-term observations at Aksengir were used to contextualize recent climate conditions and to bias-correct climate model outputs.

2.3.2. *Modelled climate data*

NASA Earth Exchange Global Daily Downscaled Climate Projections (NEX-GDDP; Thrasher et al., 2012) were used as input to the crop models. The data were obtained from the NASA Center for Climate Simulation (https://www.nccs.nasa.gov/services/data-collections/land-based-products/nex-gddp). NEX-GDDP was selected over the COordinated Regional Climate Downscaling EXperiment (CORDEX; Giorgi et al., 2009) for two reasons. First, NEX-GDDP data are available at 0.25° (~25 km) spatial resolution, compared to 0.5° (~50 km) for CORDEX (Region 8: Central Asia). Second, NEX-GDDP has been shown to provide more reliable simulations than CORDEX in other parts of Asia (e.g., Bao and Wen, 2017; Jain et al., 2019).

Four climate models – BCC-CSM1.1 (Wu et al., 2014), MIROC5 (Watanabe et al., 2010), MPI-ESM-LR (Giorgetta et al., 2013), and NorESM1-M (Bentsen et al., 2013) (Table S1) – were selected because they have demonstrated good performance with low bias relative to observational datasets in CA (Gu et al., 2015; Yu et al., 2018; Lin and Chen, 2020). Daily maximum and minimum temperatures, and precipitation from the recent-past simulations (1976–2005) and future projections (2020–2099) were used for the RCP4.5, representing low-to-medium warming, and RCP8.5, representing strong warming, scenarios. The 1976–2005 period was chosen as the 30-year baseline, as CMIP5 future climate simulations begin in 2006. Changes relative to this baseline were calculated for three time slices (2020–2049, 2040–2069, and 2070–2099) with overlapping periods in the early and mid-20th century when data are most relevant to adaptation.

Downscaled data were extracted for the four grid points closest to the experimental field (Fig. 1). Mean daily temperature was calculated by averaging daily minimum and maximum temperatures. All grid points were located at approximately the same elevation as the field. Variables were averaged across the four points and the spatially averaged series were validated against the observed Aksengir data for the baseline period. Steep elevation gradients and complex topography reduce the ability of GCMs, regional climate models, and downscaled data sets to simulate temperature and especially precipitation accurately (Shahgedanova et al., 2020). Therefore, bias correction of climate model outputs using regional meteorological observations is essential. Bias correction was applied to both baseline and future projections using Empirical Quantile Mapping (EQM), one of the most widely used correction methods (Amengual et al., 2012; Fang et al., 2015; Reiter et al., 2016).

EQM corrects the frequency distributions of simulated data to match those of observed data in the baseline period, and subsequently in future projections (Teutschbein and Seibert, 2012). The method equates the cumulative distribution functions (CDFs) of observed ($F_{o,h}$) and modelled ($F_{m,h}$) data. A bias-corrected projected value, $\hat{x}_{m,p}$ at time (t) within a projection period (p) period, was calculated following Cannon et al. (2015):

$$\hat{x}_{m,p}(t) = F_{o,h}^{-1}\{F_{m,h}[x_{m,p}(t)]\} \quad (1)$$

where the subscripts *o* and *m* denote observed and modelled data, and *h* and *p* indicate the historical and the projection periods, respectively.

Bias correction of the outputs from the selected individual climate models was performed using the R package *Qmap* (Gudmundsson, 2016), specifically the *fitQmapQUANT* function (https://CRAN.R-pr

oject.org/package=qmap). Model performance was evaluated using Taylor diagrams (Taylor, 2001), which quantify the correspondence between modelled and observed values using the Pearson correlation coefficient, Root Mean Square Error (RMSE), and standard deviation.

Bias-corrected simulations from individual climate models were used as inputs to the crop models. Ensemble means were then calculated for climate projections from the individual climate models, and for crop projections, from combinations of individual climate and crop models.

2.4. Crop data

Maize (*Skif-619* variety) was cultivated annually from 2016 to 2019, with sowing typically occurring in early May and harvesting in late October (Table 2). Vegetative growth stages were determined in the field using the leaf-count method (Hanway, 1966) in 2019. The stages used in AquaCrop and SALTMED simulations were seed, VE, V4, V6, V8, V12, R1, and R5 (Fig. S1; Table S2). Here, 'V' and 'R' denote vegetative and reproductive stages, respectively, with the accompanying numbers indicating leaf count. Harvesting was carried out using a combine harvester, and yields were measured at a weighing station and adjusted for relative water content (RWC), resulting in an average annual dry yield of 8.35 t ha^{-1} (Table 2).

To simulate crop performance, the crop growth cycle (CGC), defined as the period from sowing to physiological maturity, was calculated using thermal requirements expressed as Growing Degree Days (GDD). GDD values were derived for the emergence, initial, development, and middle-to-late growth stages (Table S3) from daily temperatures recorded at the Aksengir station, using a base temperature of 8°C which is the minimum temperature for maize growth (Allen et al., 1998). Based on a stable 10-year sowing pattern reported by local farmers, the mean sowing date was set to 8 May. The GDD values for sowing and maturity were 190°C and 1979°C, respectively, corresponding to a mean maturity date of 20 October and a mean CGC of 165 days (Table 2). This GDD-based approach was applied to both baseline and future climate scenarios to ensure consistency in model simulations.

AquaCrop requires plant density and height as input parameters (Table 1). Although the model can calculate these parameters from seed weight and sowing rate, field measurements were preferred. Density was assessed in three 10 m^2 plots (Fig. 1) once 90% of plants had emerged. Rows were spaced at 0.7 m, and a 14.3 m sowing row was marked to define each plot. Plant counts were scaled to per-hectare values. Plant height was measured at multiple growth stages using a tape measure across three plants inside three 1 m^2 randomly selected subplots within each plot (Fig. S2), and the average was used in the model.

SALTMED uses leaf area index (LAI) and surface cover fraction (SC) to represent plant density (Table 1). Both LAI and plant height were measured at each growth stage (Table S4). In 2016 and 2017, LAI was measured using PocketLAI, a smartphone app (http://www.cassandralab.com/mobiles/1). In 2019, following the app's discontinuation, LAI was calculated manually using leaf length and width measurements (Wolf et al., 1972) in each of the three 10 m^2 plots at different growth stages (Table S4). Six plants per plot were sampled, and leaf area was estimated after Lazarov (1965):

$$\mathrm{LAI} = \mathrm{length} \times \mathrm{width} \times 0.75 \quad (2)$$

where 0.75 is a coefficient standard for maize. LAI was then derived by scaling leaf area to plant density and dividing by the ground area of one hectare.

In SALTMED, crop dry matter is calculated using solar radiation, crop photosynthetic efficiency, and stress factors related to water, temperature and nitrogen levels with final yield calculated by applying a harvest index (Ragab, 2002). The optimal temperature range for net photosynthesis in maize is 28–37.5°C beyond which significant inhibition occurs (Crafts-Brandner and Salvucci, 2002). Based on these physiological thresholds, temperature thresholds were set between 0°C and 38°C.

2.5. Soil data

In AquaCrop and SALTMED, up to five and four soil layers, respectively, can be specified, with each assigned separate physical characteristics and initial soil moisture content. To characterise soil physicochemical properties (Table S5), samples were collected at the sowing stage of the 2019 growing season from three soil pits excavated to a depth of 100 cm. Samples were taken from five depth intervals (0–20, 20–40, 40–60, 60–80, and 80–100 cm). For model simulations, data from the 0–20, 20–40, and 40–60 cm layers were used (see Section 2.7).

Soil texture, defined by the proportions of sand, silt, and clay, was analysed using laser diffraction (Ryzak and Bieganowski, 2011) with a Mastersizer-v3.62 instrument (Malvern Instruments, Malvern, UK) at the University of Reading. Bulk density was determined by extracting samples of known volume with a core sampler and oven-drying them at 105°C for 24 h at the Institute of Geography and Water Security in Almaty, Kazakhstan.

Soil pH was measured by mixing 2 ml of 0.135 mol $CaCl_2$ solution with a soil sample in a 50 ml polypropylene test tube, shaking, and recording the pH after 2 min. Electrical conductivity (EC), an indicator of soil salinity, was determined at the University of Reading by measuring a 1:2.5 soil-to-deionized water solution. Organic matter (OM) content was determined by the loss-on-ignition (LOI) method: samples were oven dried at 105°C overnight and weighed (the pre-ignition weight), combusted at 500°C overnight in a muffle furnace, and reweighed (the post-ignition weight). The percentage of OM content was calculated as:

$$\%\mathrm{OM} = \frac{pre-ignition\ weight\ (g) \quad - \quad post-ignition\ weight \quad (g)}{pre-ignition\ weight\ (g)} \times 100 \quad (3)$$

This method does not result in the loss of inorganic carbon contained in $CaCO_3$ which combusts at 750 – 850 °C (Shamrikova et al., 2023). Total nitrogen was measured with a Flash Analyzer, and nitrate (NO_3^-) concentrations were determined using the hydrazine reduction method (Kamphake et al., 1967) with a San++ Automated Wet Chemistry Analyzer (Skalar).

Volumetric soil moisture was measured biweekly during the 2016–2019 growing seasons with a HydroSense II handheld soil moisture sensor (https://www.campbellsci.co.uk/hs2). Measurements were taken at three plots, with approximately nine points per plot, at 0–20 cm depth. Based on soil texture analysis, the 'silty loam' calibration setting was selected, as this was the dominant texture at 0–60 cm depth. In 2019, additional measurements were made in the three soil pits (Plots 1–3, Fig. 1) at 20 cm intervals down to 100 cm.

Table 2
Crop data for the experimental maize field (Fig. 1) including key crop management dates, plant density, irrigation supplied and measured yield. Growing season length is number of days between sowing and harvesting. The maize crop growth cycle started with sowing in May and ended with reaching maturity in October.

Cultivation year	2016	2017	2018	2019
Sowing date	10 May	5 May	3 May	14 May
Harvesting date	25 October	28 October	27 October	31 October
Number of days between sowing and harvest	168	176	177	170
Crop growth cycle (days)	163	168	170	159
Plant density (plants ha^{-1})	75,000	77000	76,000	78,000
Total irrigation amount supplied (mm)	200	240	240	260
Yield (t ha^{-1})	8.0	8.4	8.4	8.6

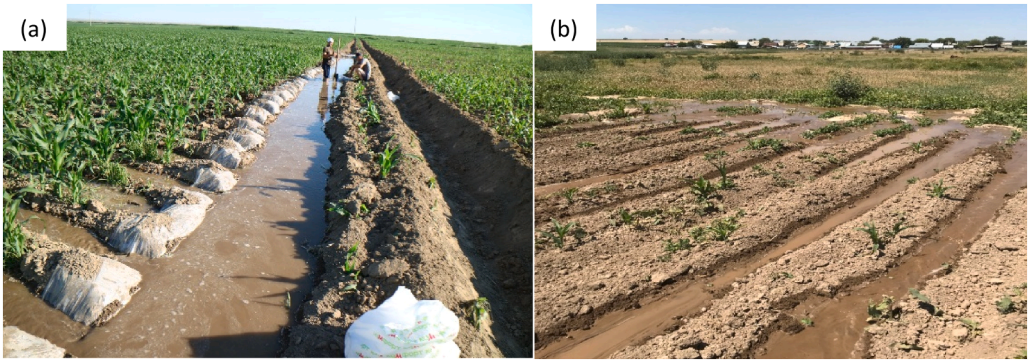

Fig. 3. (a) Furrow irrigation in the experimental field and (b) uneven water flow at the field edge.

2.6. Crop management data

Furrow irrigation, the predominant method in SEK and across CA, was applied at the experimental field (Fig. 3). Irrigation typically occurred from late June to late August, when rainfall is minimal (Fig. 2). Farmers used visual cues (e.g. soil dryness and crop wilting) to determine irrigation timing but often applied water whenever it was available in the network rather than at optimal intervals. The experimental field was generally irrigated every three to four weeks, with hoeing and ridge cultivation performed early in the season to facilitate water flow (Fig. 3).

Irrigation depth was estimated using a practical method: the time required to fill a one-litre jug was measured across five randomly selected furrows, and the average discharge rate was calculated (Duisebek, 2022). Start and end times of each irrigation event were recorded, and total volume was derived by multiplying discharge rate by duration (Table S6). SALTMED used these volumes to calculate irrigation depth per event, while AquaCrop estimated depth by dividing total volume by crop area. Quantifying furrow irrigation presents challenges due to spatial variability caused by uneven terrain, crop residues, and soil erosion (Fig. 3b), which can disrupt water distribution and introduce uncertainty.

Both models accounted for irrigation water salinity (Table 1). Water samples, collected from irrigation channels on 8 July 2019, were analysed for salinity expressed as EC of irrigation water at the Kazakhstan Institute of Geography and Water Security (Table S7).

Ammonium nitrate was applied at a rate of 150 kg N ha^{-1} annually (2016–2019) via fertigation and 1 litre ha^{-1} of MaisTer Power herbicide was used for weed control (https://www.cropscience.bayer.ru/product/maister-power). As the irrigation water was not evenly distributed across the field then the fertilisation was not homogeneous. However, given the high nitrogen and herbicide amounts, neither nitrogen limitation nor weed-induced crop stress were used in the model simulations.

For future scenario modelling, crop management inputs, including irrigation volumes and fertiliser applications, were based on the 2019 experimental year.

2.7. AquaCrop and SALTMED calibration and validation

Model calibration was performed using data from the 2019 growing season, while validation relied on data from 2016 to 2018. Input data and parameter values are summarized in Tables S4–S9. For AquaCrop, calibration involved applying conservative parameters that are broadly consistent across crops and climates (Table S8), sourced from literature and model defaults (Heng et al., 2009). For SALTMED, calibration focused on soil water content (SWC), with adjustments made to key hydraulic properties such as bubbling pressure, saturated hydraulic conductivity, saturated water content, and pore size distribution index (Table S9). Crop-related parameters (including the crop coefficient (Kc), basal crop coefficient (Kcb), effective rooting depth, and fraction cover (Fc)) were also adjusted to improve agreement between simulated and observed SWC across soil layers and with observed yields. The maximum effective rooting depth of 60 cm was applied in both models (Tables S8; S9) in line with previous studies (Peng et al., 2012; Sha et al., 2024) and successfully calibrated against the observed soil moisture, dry matter and yield. In a second step, photosynthesis efficiency was tuned to optimize biomass production and model performance.

Validation was conducting by comparing simulated SWC and final grain yield against observations for the 2016–2018 growing seasons. The same set of calibrated soil and crop parameters was applied to validation and future scenario simulations to ensure consistency.

Model performance was evaluated using five statistical metrics (Loague and Green, 1991). RMSE quantified average difference between simulations and observations:

$$RMSE = \sqrt{\frac{1}{n}\sum_{i=1}^{n}(Si - Oi)^2} \tag{4}$$

Mean Absolute Error (MAE) expressed magnitude of errors irrespective of sign:

$$MAE = \frac{1}{n}\sum_{i=1}^{n}|Si - Oi| \tag{5}$$

Relative Error (RE) expressed error as percentage of the observed value:

$$Relative\ Error\ (\%) = \left(\frac{|Oi - Si|}{Oi}\right) \times 100 \tag{6}$$

Coefficient of Residual Mass (CRM) quantified model bias whereby positive (negative) values indicated overestimation (underestimation):

$$CRM = \frac{\sum_{i=1}^{n}(Oi - Si)}{\sum_{i=1}^{n}Oi} \tag{7}$$

Coefficient of Determination (R^2) measured goodness of fit ranging from 0 (no fit) to 1 (perfect fit):

$$R^2 = \frac{\left[\sum_{i=1}^{n}(O_i - \overline{O})(S_i - \overline{S})\right]^2}{\sum_{i=1}^{n}(O_i - \overline{O})^2 \times \sum_{i=1}^{n}(S_i - \overline{S})^2} \tag{8}$$

In Eqs. 4–8, O_i is the i-th observed value, $\overline{O}$ is the mean of the observed values, $_{Si}$ is the corresponding simulated value, $\overline{S}$ is the mean of simulated values, and n the number of observed or simulated values.

3. Results

3.1. Climatic conditions and crop parameters in during the growing seasons of 2016–2019

The summers of 2017 and 2019 were warmer and drier than the 1961–2019 mean (Fig. 2). In July 2017, a positive temperature anomaly of 2.3 °C was recorded. Positive temperature anomalies of 0.9 °C, 3.3 °C, and 2.7 °C were recorded in June, July and August 2019, respectively, while precipitation was lower than the long-term average by 47, 66 and 49%, respectively although this deficit was offset using irrigation. The growing season of 2016 was colder and wetter than normal. Precipitation in May 2016 was 127 mm, exceeding the long-term monthly average by 80 mm. The growing season of 2018 was closer to the norm than the other years.

In 2019, high LAI values and above-average plant heights were recorded, with the tallest plant reaching 2.67 m, corresponding to higher temperature conditions (Table S4). The tallest crops were observed in Plot 1, which is located nearest to the irrigation water entry point (Fig. 1). Observations indicated that maize exhibited the most rapid growth following the first irrigation. Crop senescence typically began in early September.

3.2. Soil characteristics

Two soil texture types were identified: silt and silty loam (Table S5). The soil at Plot 1 (Fig. 1), located near the irrigation water entry point in the upper part of the field, had a higher silt content than Plots 2 and 3. Silty loam predominated in the lower part of the field, farther from the irrigation entry point. Soil pH ranged from 7.0 to 8.0. Organic matter content was low, varying from 1.1% to 1.4% in the top 0–20 cm layer and decreasing to below 1% in deeper layers (Table S5).

At the experimental field, irrigation water consisted of a mixture of fresh water and greywater, however, EC remained below 1 dS m^{-1} (Table S5). Notably, the plot located near the head of the furrow irrigation system exhibited higher salinity at all depths compared to the other two plots. In the lowest plot, where water distribution was less efficient, salinity increased below 60 cm. These results suggest that furrow irrigation promoted deeper salt leaching, thereby reducing salinity stress in the surface horizon.

While SOM remained relatively stable throughout the profile, nitrate concentrations decreased sharply with soil depth (Table S5). The factors and processes causing this decline in nitrate concentration are unknown and require further investigation but likely result from a combination of factors. Such factors may include the movement of nitrate ions downward with the wetting front, and possibly upwards in association with evapotranspiration and diffusion into the plant roots. Nitrification may also occur in the upper 20 cm of the soil related to a higher oxygen content whilst, at depth, higher soil moisture may promote denitrification.

3.3. AquaCrop and SALTMED calibration and validation

Calibrated parameter values are shown in Tables S8 and S9. Strong agreement between observed and simulated variables was achieved, with R^2 values exceeding 0.85 (Table 3; Fig. 4). SALTMED reproduced the temporal variability of SWC more accurately than AquaCrop, yielding higher R^2 values of 0.95 and 0.88 for the 0–20 cm and 0–60 cm soil layers, respectively, and lower CRM, RMSE, and MAE values. Simulated maize yields also closely matched observations, with SALTMED producing a lower RE (2.3%) compared to AquaCrop (3.4%) (Table 4).

Model validation indicated that both AquaCrop and SALTMED simulated SWC reasonably well during the 2017 growing season, with R^2 values of 0.83 and 0.80, respectively. In contrast, model performance was weaker in 2016, an anomalously wet year (Fig. 2), with R^2 values of 0.78 for AquaCrop and 0.77 for SALTMED (Table 3). RE for maize yield ranged from 3 to 6% for AquaCrop and 2–4% for SALTMED across the 2016–2018 growing seasons.

3.4. Simulated climate and climate projections

The simulated annual temperature cycles closely matched observations during the baseline period (Fig. 5), even before bias correction, as indicated by high correlation coefficients in the Taylor diagrams (Fig. S3). All models, however, underestimated maximum temperatures by 1.2–1.5°C and overestimated minimum temperatures by 3.9–4.2°C in JJA, with RMSE values below 5°C. Simulated precipitation also reproduced the observed annual cycle well, with correlation coefficients above 0.90 (Fig. S3). Nonetheless, all models underestimated monthly precipitation in April and May (the wettest months) and two of the four models also underestimated precipitation in August (Figs. 5, S3). These biases were effectively corrected using the EQM procedure (Fig. 5; S3).

The statistical significance of projected changes was assessed by comparing future climate model projections with the standard deviation of both modelled and observed historical data. All models projected a statistically significant increase in air temperature under both RCP (Table 5; Fig. 5). Among them, NorESM1-M indicated the strongest warming, while MPI-ESM projected the smallest increase in both maximum and minimum temperatures across all time slices and scenarios (Figs. S4, S5). Most models suggested stronger warming during December–February (DJF), followed by JJA, relative to the transitional seasons.

Relative changes in precipitation are presented in Table 5 and Figure S5. On average, growing-season precipitation was projected to either increase by up to 10% or remain unchanged, except toward the end of the 21st century when a decline of around 10% was projected under RCP 8.5. However, these mean values mask considerable variability, with individual model projections ranging from a 40% reduction to a 30% increase in May–September precipitation. This inter-model spread was particularly pronounced under RCP4.5, where no clear consensus emerges on the direction of change (Fig. S4). As a result of insignificant trends in precipitation, the aridity index (AI), defined as a

Table 3
Model performance metrics for soil water content (SWC) calibration using data of the 2019 growing season and validation using data of the 2016 and 2017 growing seasons.

Metrics	Soil depth 0–20 cm						Soil depth 0–60 cm	
	2016		2017		2019		2019	
	Aqua-Crop	SALTMED	Aqua-Crop	SALTMED	Aqua-Crop	SALTMED	Aqua-Crop	SALTMED
R^2	0.78	0.77	0.80	0.83	0.86	0.95	0.85	0.88
CRM	0.079	-0.019	0.068	-0.01	0.053	-0.014	-0.05	-0.018
RMSE	0.031	0.027	0.032	0.025	0.049	0.012	0.030	0.011
MAE	0.03	0.022	0.027	0.021	0.033	0.011	0.023	0.010

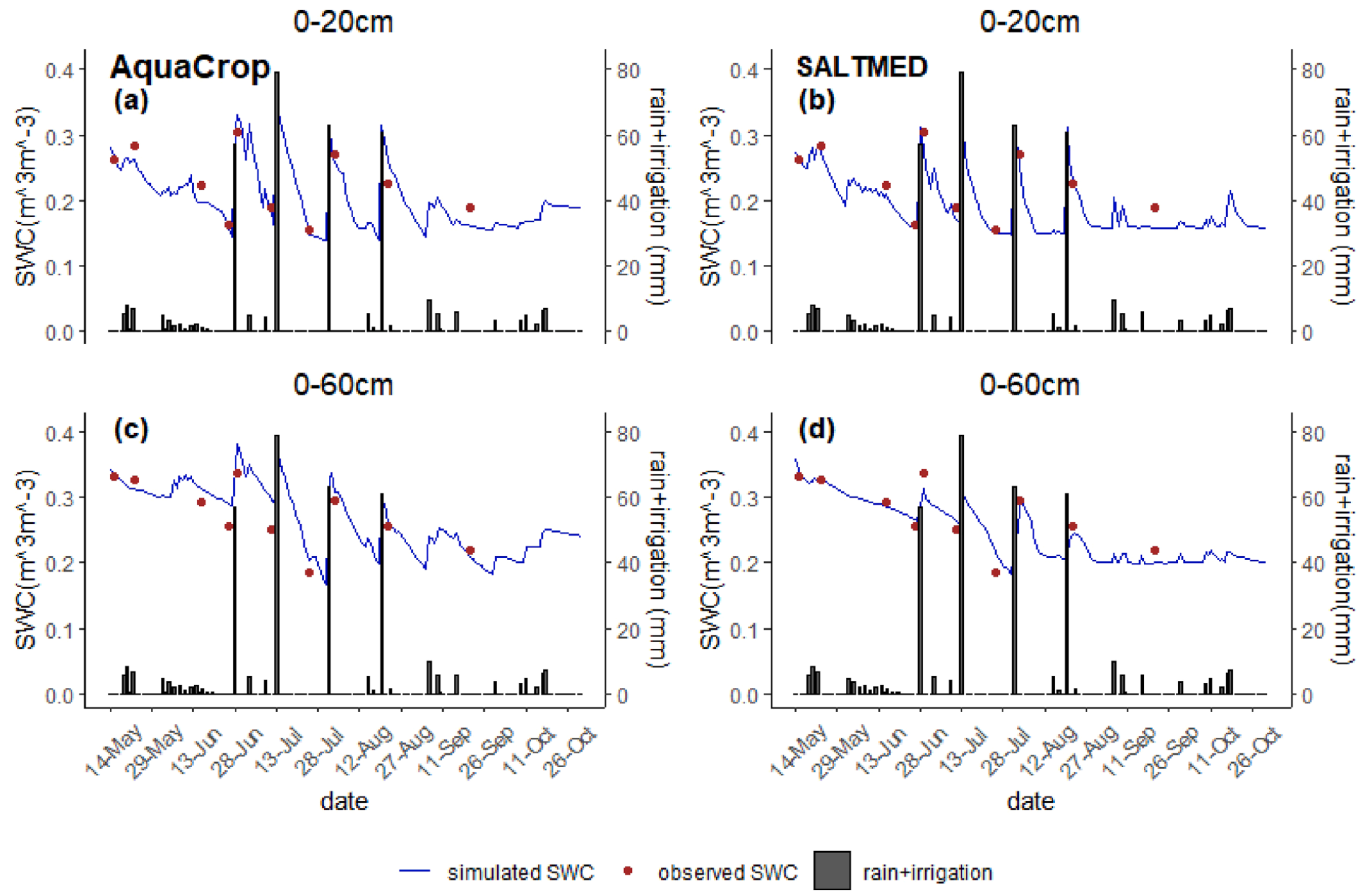

Fig. 4. Observed and simulated SWC ($m^3\ m^{-3}$) as in 2019 by AquaCrop (a, c) and by SALTMED (b, d) for the 0–20 cm and lumped 0–60 cm layers of soil. The vertical bars show water depth from rain and irrigation.

Table 4
Observed and simulated maize yields and relative errors (RE) during the 2016–2018 validation and 2019 calibration growing seasons.

Year	Observed	AquaCrop		SALTMED	
		Simulated	RE (%)	Simulated	RE (%)
2016	8.0	8.4	5.0	8.3	3.7
2017	8.4	8.9	5.9	8.7	3.5
2018	8.4	8.8	4.7	8.6	2.3
2019	8.6	8.9	3.4	8.8	2.3

ratio between precipitation and potential evaporation (Table 6), did not exhibit a strong change as confirmed by global studies (Greve et al., 2019) although currently, the AI value of 0.21 correspond to the semi-arid area and the 2070–2099 value of 0.19 corresponding to arid climate (Zomer et al., 2022).

Changes in extreme temperature events, such as frost (minimum temperature < 0°C) and heat stress (maximum temperature > 38°C), were assessed under future climate scenarios (Table S10). In the baseline climate (1976–2005), the number of days with minimum temperatures below 0°C averaged 6.7 in April and 0.7 in May. By 2070–2099 under RCP8.5, these cold days were projected to decline to zero in both months. By contrast, days with maximum temperatures exceeding 38°C in July and August, which averaged 2.5 and 1.9 days, respectively, in the baseline period, were projected to rise sharply, reaching 25 days in July and 24 days in August by the end of the century under RCP8.5.

3.5. Projected future changes the length of growing cycle, water use and yields

The mean projected changes in CGC, CWR, and maize yields are presented in Table 6. These values were calculated by averaging outputs from AquaCrop and SALTMED simulations driven by individual climate model projections (Figs. 6 and 7). The CGC was projected to decrease from the current 159–170 days to 127–129 days under RCP4.5 and to 120–123 days under RCP8.5 in 2070–2099, representing a reduction of 36–38 and 42–45 days, respectively. Both AquaCrop and SALTMED produced very similar results. Even in the nearer-term period of 2020–2049, which is particularly relevant for adaptation planning, CGC is expected to decline by approximately 20 days under RCP4.5 and by 30 days under RCP8.5. Sowing dates were projected to shift from the first two weeks of May to the last week of April in 2020–2069, and to the middle of April in 2070–2099 (Table 6).

This shortening of CGC resulted in a reduced CWR, simulated to decline by 11–15% in AquaCrop and 16–24% in SALTMED over the 21st century (Table 6; Fig. 6). Simulated future maize yields also showed a decreasing trend across the 2020–2100 period, with reductions of between 6–11% and 3–7% projected by AquaCrop and SALTMED, respectively (Table 6; Fig. 7). While SALTMED simulated a greater reduction in CWR, AquaCrop projected more substantial decreases in yield.

Water productivity, calculated as a ratio of modelled yield to the sum of modelled crop water requirement (CWR) and rainfall, ranged between 11.0 kg ha^{-1} mm^{-1} (SALTMED) and 12.5 kg ha^{-1} mm^{-1} (AquaCrop) for the 2020–2049 period. The largest projected increase (+10%) was simulated by SALTMED under the RCP8.5 scenario for 2070–2099 (Table S11).

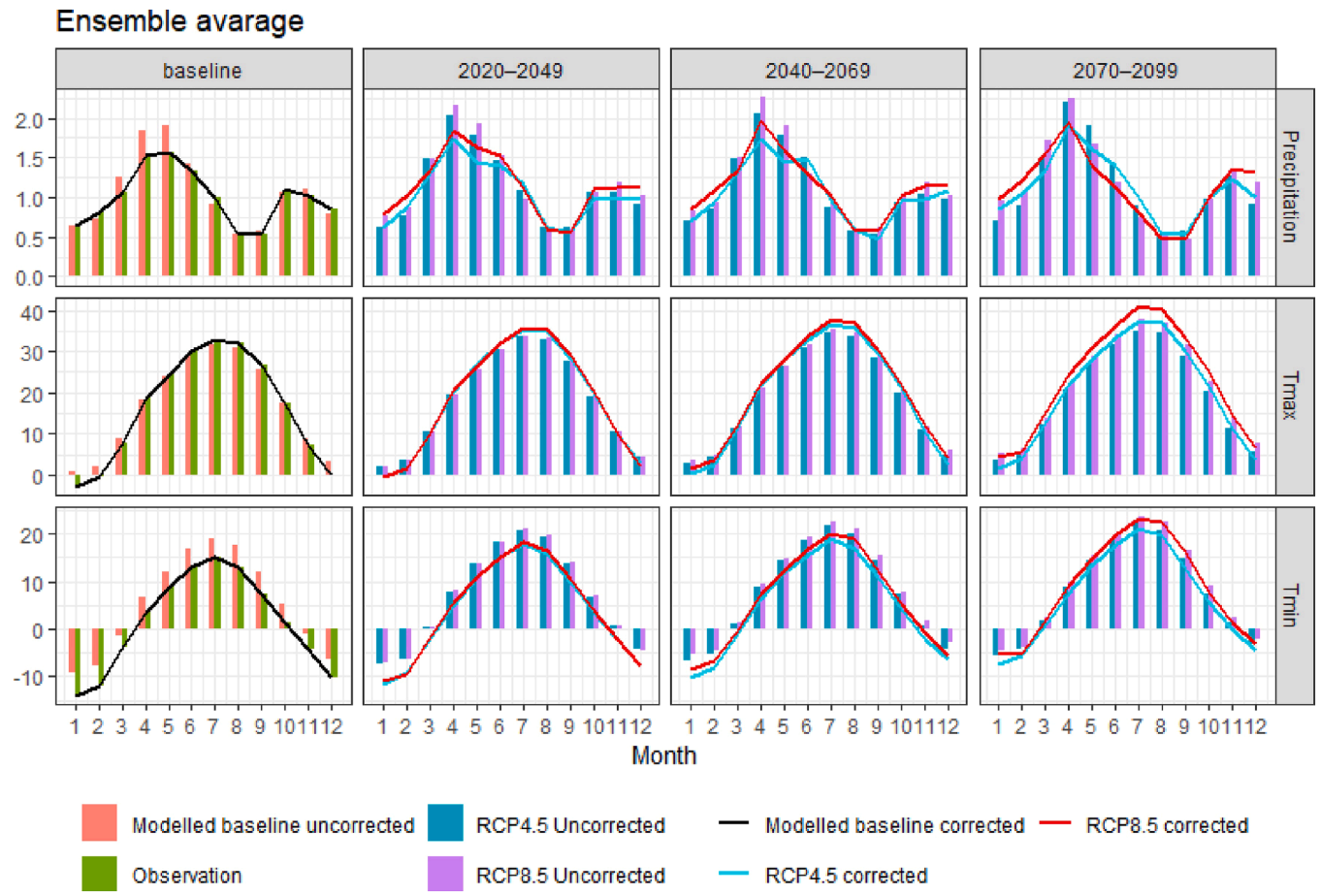

Fig. 5. Observed, simulated uncorrected and bias-corrected ensemble-average values of precipitation intensity (mm day^{-1}), maximum (Tmax) and minimum (Tmin) temperature (°C) for the baseline climate (1976–2005) and for the 2020–2049, 2040–2069, and 2070–2099 time slices for RCP 4.5 and RCP 8.5 scenarios. The simulation domain is shown in Fig. 1.

Table 5
Projected changes, based on the bias-corrected data, in maximum (Tmax) and minimum (Tmin) air temperatures and relative changes in precipitation intensity (PI; expressed as a ratio between future and baseline precipitation) in comparison with the baseline period (1976–2005) for the growing season (May to September). The numbers in bold represent the ensemble-averaged values, while the ranges show the spread of projections from individual model simulations.

RCP / time slice	RCP 4.5			RCP 8.5		
	Tmax (°C)	Tmin (°C)	PI	Tmax (°C)	Tmin (°C)	PI
2020–2049	**2.3** (1.7–2.9)	**2.4** (1.8–2.5)	**1.1** (0.9–1.3)	**2.4** (1.8–2.8)	**2.8** (2.0–3.1)	**1.1** (1.0–1.2)
2040–2069	**3.2** (2.5–4.0)	**3.4** (2.7–3.8)	**1.0** (0.8–1.2)	**4.0** (3.4–4.4)	**4.6** (3.8–5.1)	**1.1** (0.9–1.3)
2070–2099	**3.9** (3.2–4.4)	**5.3** (3.3–9.4)	**1.0** (0.7–1.2)	**6.9** (6.5–7.4)	**7.8** (7.1–8.1)	**0.9** (0.6–1.0)

4. Discussion

4.1. Simulated effects of projected changes in climate on maize cultivation

Climatic warming in SEK has already been observed, with maximum summer temperatures increasing by 0.27°C per decade between 1961 and 2019. Future projections (Table 5; Fig. S4) indicate continued warming beyond maize's physiological optimum, with days exceeding the critical 38°C threshold (Herrero and Johnson, 1980) projected to increase fourfold in the 2020–2049 period compared to the baseline and to occur almost daily by the end of the century (Table S10). While a decline in the frequency of frost days during April–May may benefit germination, the negative effects of extreme summer heat will dominate.

Model experiments with a late-maturing maize variety (159–170 day CGC) projected yield reductions under both scenarios ranging between -5.6% and -11.6% in AquaCrop and -4.5% and -8.1% in SALTMED across the time slices (Table 6). These declines are primarily temperature-driven, as irrigation was held constant. A pronounced shortening of the crop growth cycle from approximately 165 days (2016–2019) through 127–140 days in 2020–2049120–129 days in 2070–2099 was projected, consistent with global observations of accelerated phenology under warming conditions (Lobell et al., 2011; Bassu et al., 2014; Jägermeyr et al., 2021). Shorter CGCs will lead to a decrease in CWR by 11–15% in AquaCrop and 16–24% in SALTMED by 2100 and it will be more pronounced in the second half of the 21st century according to the SALTMED simulations (Table 6). The projected decline in CWR and associated small increase in water productivity (Table S11) suggest that less irrigation water will be required during the crop growth cycle

Table 6
Projected changes in maize yield, CGC, and CWR under different climate scenarios. In the future scenarios, values represent means of simulations driven by individual climate models; ranges indicate medians of individual simulations (Figs. 6 and 7). CWR, rainfall, and reference evapotranspiration (ETo) correspond to the CGC from sowing to maturity. Observed rainfall and irrigation values are shown for 2016–2019.

Scenario	Period	Sowing date	CGC (days)	Simulated yield (t ha^{-1})	Yield relative change (%)	CWR (mm)	CWR relative change (%)	Rainfall (mm)	Irrigation (mm)	Rainfall + irrigation (mm)	ETo (mm)
AquaCrop											
	2016	08 May	163	8.4		542		260	200	460	739
	2017	05 May	166	8.9		597		104	240	344	787
	2018	03 May	170	8.8		570		120	240	360	796
	2019	13 May	159	8.9		586		107	260	367	864
RCP4.5	2020–2049	01 May	148	8.4	-5.6 (-7.8 – −3.8)	505	-12 (-28.2 – −2.1)	167	260	427	813
	2040–2069	27 Apr	132	8.2	-8.1 (-9.2 – −7.2)	499	-14 (-32.2 – −1.8)	154	260	414	821
	2070–2099	23 Apr	129	8.0	-10.1 (-11.3 – −9.3)	504	-13 (-35.2 – −5.8)	161	260	421	814
RCP8.5	2020–2049	27 Apr	138	8.3	-6.7 (-8.7 – −4.9)	511	-11 (-29.8 – −3.9)	175	260	435	809
	2040–2069	22 Apr	130	8.1	-9.3 (-10.1 – −9.0)	512	-11 (-27.9 – −0.1)	168	260	428	831
	2070–2099	17 Apr	123	7.9	-11.6 (-13.6 – −10.3)	489	-15 (-34.2 – −4.0)	148	260	408	774
SALTMED											
	2016	08 May	163	8.3		615		260	200	460	733
	2017	05 May	166	8.7		781		104	240	344	826
	2018	03 May	170	8.6		659		120	240	360	791
	2019	13 May	159	8.8		756		107	260	367	893
RCP4.5	2020–2049	30 Apr	140	8.5	-4.5 (-4.8 – −3.6)	591	-16 (-23.8– −12.1)	167	260	427	816
	2040–2069	26 Apr	134	8.4	-5.4 (-5.1 – −5.7)	581	-17 (-25.0 – −15.1)	154	260	414	807
	2070–2099	23 Apr	127	8.3	-6.8 (-8.0 – −6.2)	565	-19 (-27.8 – −20.6)	161	260	421	800
RCP8.5	2020–2049	29 Apr	138	8.4	-5.1 (-5.9 – −4.5)	587	-16 (-26.4 – −11.7)	175	260	435	813
	2040–2069	24 Apr	127	8.3	-6.5 (-6.8 – −5.9)	568	-20 (-30.9 – −18.4)	168	260	428	787
	2070–2099	17 Apr	120	8.2	-8.1 (-8.4 – −7.2)	531	-24 (-37.1 – −27.3)	148	260	408	768

overall rather than more. However, uncertainties in precipitation projections contribute directly to uncertainties in projected water productivity. The global mean water productivity for maize has been estimated at 18.6 kg ha^{-1} mm^{-1}, with values ranging from 8.0 to 33.2 kg ha^{-1} mm^{-1} (Zheng et al., 2018). Results of this study showed that both current (2016–2019; Table 6) and projected values (Table S11) fall at the lower end of this global range.

Statistical significance of the projected yield reductions can be assessed by comparing the projected changes with the standard deviations of observed yields. For AquaCrop, the projected reductions were significant across both scenarios and all time slices. In contrast, SALTMED projected smaller reductions, which become significant in the late century under RCP4.5 and in the mid-century under RCP8.5. However, this assessment is limited by the short observational yield record, as farmers generally do not maintain long-term yield data.

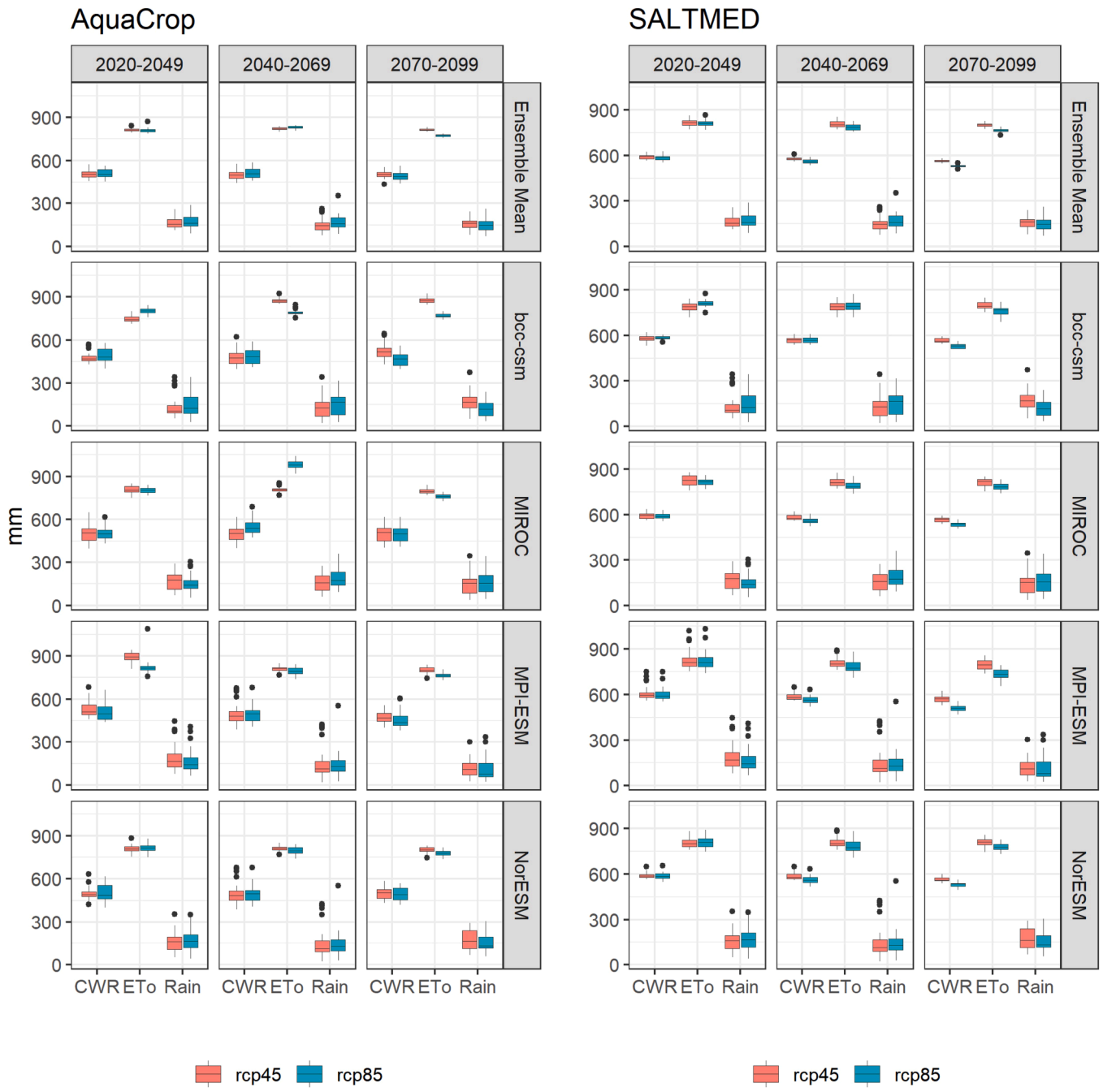

Fig. 6. Boxplots of Crop Water Requirement (CWR), Reference Evapotranspiration (ETo), and rainfall for the 2020–2049, 2040–2069, and 2070–2099 time slices as simulated using AquaCrop and SALTMED for RCP4.5 and RCP8.5 scenarios.

4.2. Uncertainty and limitations of the model-based assessment

Uncertainty in projections arises from differences in crop model structure, heat stress representation, climate scenarios, and spatial scope of the study. Global crop model intercomparison projects showed that crop models introduce more variability in yield projections than climate models (Rosenzweig et al., 2014; Jägermeyr et al., 2021) and simulated maize yields can vary by a factor of two across crop models even under baseline conditions (Bassu et al., 2014). While our study employed multiple GCMs for climate projections, similar to Jägermeyr et al. (2021), it relied on only two crop models. AquaCrop and SALTMED diverged more in their yield and water requirement projections than RCP4.5 and RCP8.5 did from each other. AquaCrop's dynamic crop coefficient (Kc) approach produced a wider range of outcomes than SALTMED's stage-specific Kc (Table 6; Figs. 6–7), illustrating how parameterisation choices shape results. In the future, Kc values are not expected to change substantially as shown by Tegegne et al. (2025) as both ETo and ETa are projected to increase at comparable rates.

Crop–water models may underestimate yield losses under extreme heat. Empirical studies suggest that the observed impacts are often more severe than those in model simulations (Liu et al., 2014). Simplified representations of photosynthesis, light-use efficiency, transpiration, and nutrient constraints limit model accuracy (Rosenzweig et al., 2013; Stocker et al., 2020). Moreover, shorter CGCs imply reduced solar radiation capture and photosynthesis (Bassu et al., 2014), a process not explicitly modelled here. Future work, therefore, should include more physiologically detailed models.

Recent comparisons between harmonized crop–water model

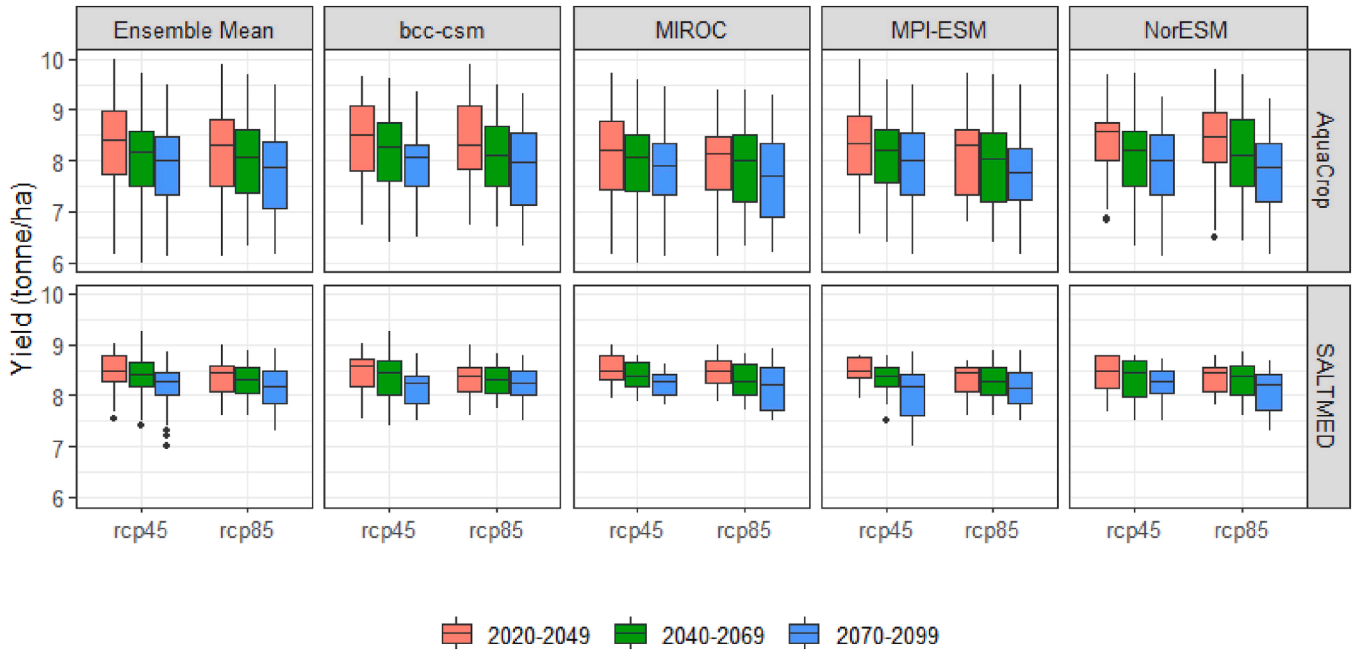

Fig. 7. Boxplots of maize yield for the 2020–2049, 2040–2069, and 2070–2099 time slices as simulated by AquaCrop and SALTMED for RCP4.5 and RCP8.5 scenarios.

projections based on CMIP5 and CMIP6 data have demonstrated that the ensemble response of the new generation of crop and climate models to RCP2.6 (SSP1–2.6) and RCP8.5 (SSP5–8.5) forcing is more pronounced under CMIP6 (Jägermeyr et al., 2021). Specifically, for maize, the mean projected global productivity reduction for the 2070–2099 period was approximately 10% (SSP1–2.6) and 20% (SSP5–8.5) greater when using CMIP6 projections compared to CMIP5 due to an earlier onset and intensification of climate change impacts. Expanding the crop–water model ensemble and incorporating CMIP6-based scenarios would, therefore, enhance the robustness of future crop projections in SEK.

Inconsistencies among precipitation projections from different models are a well-documented issue in CA, where both the magnitude and direction of projected trends often diverge. This problem was particularly pronounced in the CMIP5 ensemble (Huang et al., 2014), from which the projections used in this study were derived. In the study area, projected changes in growing-season precipitation range from a 40% reduction to a 30% increase (Table 5). Although CMIP6 models show improved consistency projecting an increase in annual precipitation in the northern part of CA and in the Tien Shan mountains, the issue has not been fully resolved (Jiang et al., 2020). In our simulations, applying irrigation at 2019 levels moderated the effects of these inconsistencies on yields, but it did not eliminate the uncertainty surrounding future irrigation water availability.

Finally, the presented simulations were based on the observational data from an individual farm. Even within the farm, crop characteristics varies (e.g., crop heights varied between the plots depending on the distance to the irrigation water entry point) that is a limitation of the study. Broader spatial replication, reflecting the diversity of growing conditions and crop characteristics, as well as hydrological integration are needed to capture regional heterogeneity and water-availability dynamics.

4.3. Comparison with other model-based assessments

The negative effects of rising temperatures and drought on maize productivity have been documented in experimental (Hatfield and Prueger, 2015), observational (Lobell et al., 2011, 2014), and modelling studies (Bassu et al., 2014) worldwide. Timlin et al. (2024) estimated that global maize yields will decline by approximately 7.4% for every 1°C increase in global mean temperature, although the magnitude of this effect varied by region. Water availability is another major determinant of yield: insufficient rainfall, particularly when drought coincides with sensitive growth stages, exacerbates yield losses (Lobell et al., 2011) although reductions are generally smaller in irrigated systems (Ray et al., 2015, 2019). A recent Global Gridded Crop Model Intercomparison projected global maize yield reductions of about 6% under SSP1–2.6 and 24% under SSP5–8.5 by 2100 (Jägermeyr et al., 2021), with consistent patterns across models and major producing regions such as North America, Mexico, west Africa, Central Asia, and China. Irrigated maize yields were projected to decrease by 13–19% and by 16% in northern (Tao and Zhang, 2010) and in north-western (Gao et al., 2024) China, respectively, by the end of the 21st century. A 17% reduction in irrigated maize yield was projected for Portugal (Yang et al., 2017). Rainfed maize yields in the U.S. Corn Belt were projected to decline by 18% by the end of the 21st century, primarily due to an increase of more than 5 °C in growing-season temperature (Ummenhofer et al., 2015). In the south-eastern United States, yields could decrease by 4.6% per °C (Cammarano and Tian, 2018).

Our simulations align with this global evidence but show smaller yield reductions for SEK, where maize is irrigated. By 2070–2099 under RCP8.5, AquaCrop and SALTMED project yield reduction of 11.6% and 8.1%, respectively (Table 6). Irrigation not only ensures water supply but can also reduce canopy and near-surface air temperatures, mitigating heat stress (Sacks et al., 2009) as well as VPD, improving pollen moisture content and, therefore, viability (Fonseca and Westgate, 2005). The projected shortening of the crop growing cycle (CGC) by 36–38 days under RCP4.5 and 42–45 days under RCP8.5 by 2100 (Table 6) aligns with global (Jägermeyr et al., 2021) and regional projections (Tao and Zhang, 2010; Yang et al., 2017), though it exceeds the approximately 10-day reduction projected for north-western China for a maize variety with a 112–115-day CGC (Gao et al., 2024).

In CA, the growing season has already shortened by approximately 0.9 days yr^{-1} between 2000 and 2019, particularly in central and western Kazakhstan and the Syr Darya basin (Wu et al., 2021). Similar contractions have been reported elsewhere: reductions of 66 days in north-eastern China (Lin et al., 2017), 50 days in warmer climates such

as Morocco (Bouras et al., 2019), and 4.8 days per decade globally (Liu et al., 2013). Together with our model outputs, these results highlight a consistent global pattern of maize phenological acceleration and growing-season contraction under future warming scenarios.

4.4. Regional water availability and recommendations for adaptation

Irrigation underpins agriculture in CA, consuming over 80% of water withdrawals, most sourced from snow and glacier melt (Cai et al., 2003). Ongoing glacier retreat and altered runoff seasonality threaten this supply in SEK (Shahgedanova et al., 2020) and across CA (Hock et al., 2019). Currently, runoff is increasing in glacierized catchments, but peak water is expected around the 2040 s. Summer flows will decline thereafter and seasonal maximum in runoff, supported by snow melt, will shift towards spring (Hock et al., 2019; Shahgedanova et al., 2020). The use of treated (grey) wastewater is currently limited to areas near large cities, such as Sorkol Lake near Almaty (Mamadiyarov et al., 2015; Yapiyev et al., 2021). Its application should be expanded; however, this water has a higher salinity (470 ppm TDS) compared with water supplied by snow and glacier melt (70–210 ppm TDS; Wade et al., 2024). Reservoirs storing both melt and treated water can buffer seasonal shifts, but increased evaporation under warming will limit their effectiveness (Yapiyev et al., 2017). In addition, current irrigation infrastructure is deteriorating, reducing farmers' capacity to benefit from present increases in meltwater in glacierized catchments (Thevs et al., 2017; Barrett et al., 2017; Shahgedanova et al., 2018).

Shorter growing cycles and potential increases in spring precipitation could partially reduce irrigation demand in SEK, consistent with global projections of a 17% reduction by the 2080 s (Konzmann et al., 2013) and with projections for north-western China by Song et al. (2019). However, furrow irrigation currently used in the region is inefficient and vulnerable to evaporative losses. Moreover, there is uncertainty about the projected decrease in irrigation demand. Thus, projections for north-western China by Gao et al. (2024) showed an increase in evapotranspiration and a greater demand for water for maize in the future despite shortening CGC. Replacing furrow irrigation with more efficient systems such as sprinkler or drip and improving water scheduling could enhance water-use efficiency and reduce risks of either excessive water uses under lower CRW as projected for SEK, or higher evaporative losses as projected for China (Thevs et al., 2017).

Adaptation strategies such as earlier sowing and shorter-maturing cultivars can help align crop water demand with annual maxima in rainfall and runoff (Tao and Zhang, 2010; Bassu et al., 2014). Saddique et al. (2020) showed that adjusting sowing dates, together with modified irrigation, could offset a projected 33% reduction in maize yields in China and instead achieve a 2–31% increase. However, frost risk in SEK remains significant in April even at the end of the 21st century under both RCP scenarios (Table S10), and changes in sowing dates and cultivar selection must account for the probability of spring frosts, tolerance to high temperatures, and traits such as early-morning pollen shedding (Dhillon et al., 1988; Tao and Zhang, 2010; Barlow et al., 2015). Varieties that shed pollen in the early morning, when temperatures are cooler, offer an additional adaptation strategy to heat stress (Shah et al., 2011).

Limited adaptive capacity of small and medium-sized farms remains a barrier to adaptation in SEK, underscoring the need for targeted support and knowledge transfer (Barrett et al., 2017; Murzakulova et al., 2019). As a result, disseminating crop–water modelling results to farmers and policymakers can inform irrigation planning, cultivar choice, agronomic practices, and broader adaptation practices.

5. Conclusion

This study used the AquaCrop and SALTMED crop–water models, calibrated with field data from south-eastern Kazakhstan, to assess how projected climate change will affect maize growth, yield, and water requirements in a cryosphere-dependent agricultural region. Bias-corrected outputs from four climate models under RCP4.5 and RCP8.5 scenarios showed that increasing temperatures will substantially shorten the maize growth cycle by up to 42–45 days by 2100. As a result, crop water requirements will decline by 11–15% (AquaCrop) and 16–24% (SALTMED), while yields are projected to fall by up to 11.6% and 8.1%, respectively. These changes are driven primarily by rising temperatures and accelerated phenology rather than changes in precipitation, which show no clear trend.

While irrigation moderates yield losses, glacier retreat and shifting runoff patterns will challenge future water availability. Adaptation strategies such as earlier sowing, selecting shorter-maturing and heat-tolerant cultivars, and replacing inefficient furrow irrigation with more efficient systems could help sustain yields and improve water-use efficiency. Future work should use crop–water models that explicitly represent photosynthesis and evapotranspiration to better assess the impact of reduced solar radiation capture on yields and incorporate changing water availability due to the degradation of the cryosphere. Such analyses will support the development of robust adaptation strategies and inform climate-resilient agricultural planning in Central Asia.

CRediT authorship contribution statement

Baktybek Duisebek: Writing – review & editing, Visualization, Investigation, Formal analysis. **Maria Shahgedanova:** Writing – original draft, Supervision, Project administration, Funding acquisition, Conceptualization. **Andrew J. Wade:** Writing – original draft, Supervision, Conceptualization. **Ragab Ragab:** Writing – review & editing, Supervision. **Zarina Saidaliyeva:** Visualization, Investigation. **Nikolay Kasatkin:** Investigation.

Declaration of Competing Interest

The authors confirm that there are no competing interests.

Acknowledgement

The authors are grateful to Mr Alexey Gorbatyuk who kindly allowed us to use his farm as the experimental site and provided a wealth of information supporting this project. The field work in 2016–2017 and in 2018–2019 was supported by the UK – Kazakhstan Newton – al Farabi Fund (Grant No 172722855, 'Climate Change, Water Resources and Food Security in Kazakhstan') and the Global Challenges Research Fund (Grant No GCRFNGR3\1389, 'CARAWAN: Central Asia Research and Adaptation Network'). Duisebek was supported by the Bolashak International Scholarship awarded by Government of Kazakhstan while studying for PhD at the University of Reading. The AWS data were provided by the Tuyuksu Mountain Observatory run by the Central Asia Regional Glaciological Centre under the Auspices of UNESCO. The authors are grateful to Dr Dolgikh, Kazakhstan National Hydrometeorological Service, for supplying the Askengir station data; to Dr. Azamat Madibekov, Head of the Laboratory of Hydrochemistry and Environmental Toxicology at Institute of Geography and Water Security, Almaty, Kazakhstan, for providing laboratory facilities to facilitate the soil measurements; and Prof. Martin Lukac, University of Reading, for valuable discussions and suggestions. We also thank the anonymous reviewers whose comments helped us to improve the manuscript.

Appendix A. Supporting information

Supplementary data associated with this article can be found in the online version at doi:10.1016/j.agwat.2026.110343.

Data availability

The key data are available in the Supplementary Material.

References

Akhtar, F., Tischbein, B., Awan, U.K., 2013. Optimizing deficit irrigation scheduling under shallow groundwater conditions in lower reaches of Amu Darya River Basin. Water Resour. Manag. 27 (10), 3165–3178.

Allen, R.G., Pereira, L.S., Raes, D., Smith, M., 1998. Crop evapotranspiration: Guidelines for computing crop water requirements. In: FAO Irrigation and Drainage Paper No, 56. FAO, Rome. ⟨https://www.fao.org/4/x0490e/x0490e00.htm⟩ (Available at).

Amengual, A., Homar, V., Romero, R., Alonso, S., Ramis, C., 2012. A statistical adjustment of regional climate model outputs to local scales: application to Platja de Palma, Spain. J. Clim. 25 (3), 939–957.

Bao, Y., Wen, X., 2017. Projection of China's near-and long-term climate in a new high-resolution daily downscaled dataset NEX-GDDP. J. Meteorol. Res. 31 (1), 236–249.

Barlow, K.M., Christy, B.P., O'Leary, G.J., Riffkin, P.A., Nuttall, J.G., 2015. Simulating the impact of extreme heat and frost events on wheat crop production: a review. Field Crops Res. 171, 109–119.

Barrett, T., Feola, G., Khusnitdinova, M., Krylova, V., 2017. Adapting agricultural water use to climate change in a post-Soviet context: Challenges and opportunities in Southeast Kazakhstan. Hum. Ecol. 45 (6), 747–762.

Bassu, S., Brisson, N., Durand, J.L., Boote, K., Lizaso, J., Jones, J.W., Rosenzweig, C., Ruane, A.C., Adam, M., Baron, C., Basso, B., 2014. How do various maize crop models vary in their responses to climate change factors? Glob. Change Biol. 20 (7), 2301–2320.

Beck, H., Zimmermann, N., McVicar, T., Vergopolan, N., Berg, A., Wood, E.F., 2018. Present and future Köppen-Geiger climate classification maps at 1-km resolution. Sci. Data 5, 180214.

Bentsen, M., Bethke, I., Debernard, J.B., Iversen, T., Kirkevåg, A., Seland, Ø., Drange, H., Roelandt, C., Seierstad, I.A., Hoose, C., Kristjánsson, J.E., 2013. The norwegian earth system model, NorESM1-M — Part 1: description and basic evaluation of the physical climate. Geosci. Model Dev. 6 (3), 687–720.

Bobojonov, I., Aw-Hassan, A., 2014. Impacts of climate change on farm income security in Central Asia: an integrated modeling approach. Agric. Ecosyst. Environ. 188, 245–255.

Bouras, E., Jarlan, L., Khabba, S., Er-Raki, S., Dezetter, A., Sghir, F., Tramblay, Y., 2019. Assessing the impact of global climate changes on irrigated wheat yields and water requirements in a semi-arid environment of Morocco. Sci. Rep. 9 (1), 1914.

Cai, X., McKinney, D.C., Rosegrant, M.W., 2003. Sustainability analysis for irrigation water management in the Aral Sea region. Agric. Syst. 76 (3), 1043–1066.

Çakir, R., 2004. Effect of water stress at different development stages on vegetative and reproductive growth of corn. Field Crops Res. 89 (1), 1–16.

Cammarano, D., Tian, D., 2018. The effects of projected climate and climate extremes on a winter and summer crop in the southeast USA. Agric. For. Meteorol. 248, 109–118.

Cannon, A.J., Sobie, S.R., Murdock, T.Q., 2015. Bias correction of GCM precipitation by quantile mapping: how well do methods preserve changes in quantiles and extremes? J. Clim. 28 (17), 6938–6959.

Challinor, A.J., Watson, J., Lobell, D.B., Howden, S.M., Smith, D.R., Chhetri, N., 2014. A meta-analysis of crop yield under climate change and adaptation. Nat. Clim. Change 4 (4), 287–291.

Crafts-Brandner, S.J., Salvucci, M.E., 2002. Sensitivity of photosynthesis in a C4 plant, maize, to heat stress. Plant Physiol. 129 (4), 1773–1780.

Dhillon, B.S., Sharma, R.K., Malhotra, V.V., Khehra, A.S., 1988. Evaluation of maize germplasm for tolerance to low temperature stress under field and laboratory conditions. J. Agron. Crop Sci. 160 (2), 89–93.

Duisebek, B., 2022. Modelling Impacts of Climate Change on Maize Production in South-eastern Kazakhstan. Unpublished Phd thesis. University of Reading, UK. https://doi.org/10.48683/1926.00116542.

Eisfelder, C., Klein, I., Niklaus, M., Kuenzer, C., 2014. Net primary productivity in Kazakhstan, its spatio-temporal patterns and relation to meteorological variables. J. Arid Environ. 103, 17–30.

Fallah, B., Didovets, I., Rostami, M., Hamidi, M., 2024. Climate change impacts on Central Asia: trends, extremes and future projections. Int. J. Climatol. 44 (10), 3191–3213.

Fang, G.H., Yang, J., Chen, Y.N., Zammit, C., 2015. Comparing bias correction methods in downscaling meteorological variables for a hydrologic impact study in an arid area in China. Hydrol. Earth Syst. Sci. 19 (6), 2547–2559.

FAO, 2017. AquaCrop training handbooks. Book I: Understanding AquaCrop, 52. Food and Agriculture Organization of the United Nations, Rome. ⟨https://openknowledge.fao.org/handle/20.500.14283/cc2380en⟩ (Available at).

FAO, 2025. Development of Small Family-Based Agricultural Producers in the Republic of Kazakhstan. Assessment Report and Public Policy Recommendations. Food and Agriculture Organization of the United Nations, Budapest. ⟨https://openknowledge.fao.org/items/43cffd4c-6f6a-4e0d-9769-65ceb6cd2a56⟩.

Farinotti, D., Longuevergne, L., Moholdt, G., Duethmann, D., Mölg, T., Bolch, T., Vorogushyn, S., Güntner, A., 2015. Substantial glacier mass loss in the Tien Shan over the past 50 years. Nat. Geosci. 8 (9), 716–722.

Fay, M., Block, R.I., Ebinger, J.O. (Eds.), 2010. Adapting to Climate Change in Eastern Europe and Central Asia, 180. World Bank, Washington, DC.

Fonseca, A.E., Westgate, M.E., 2005. Relationship between desiccation and viability of maize pollen. Field Crops Res. 94 (2-3), 114–125.

Gao, X., Liu, J., Lin, H., Wen, Y., Chen, R., Javed, T., Mu, X., Wang, Z., 2024. Temperature increase may not necessarily penalize future yields of three major crops in Xinjiang, Northwest China. Agric. Water Manag. 304, 109085.

Giorgetta, M.A., Jungclaus, J., Reick, C.H., Legutke, S., Bader, J., Böttinger, M., Brovkin, V., Crueger, T., Esch, M., Fieg, K., Glushak, K., 2013. Climate and carbon cycle changes from 1850 to 2100 in MPI-ESM simulations for CMIP5. J. Adv. Model. Earth Syst. 5 (3), 572–597.

Giorgi, F., Jones, C., Asrar, G.R., 2009. Addressing climate information needs at the regional level: the CORDEX framework. WMO Bull. 58 (3), 175. ⟨https://cordex.org/wp-content/uploads/2012/11/cordex_giorgi_wmo-1.pdf⟩ (Available at).

Greve, P., Roderick, M.L., Ukkola, A.M., Wada, Y., 2019. The aridity Index under global warming. Environ. Res. Lett. 14, 124006.

Groisman, P., Shugart, H., Kicklighter, D., Henebry, G., Tchebakova, N., Maksyutov, S., Monier, E., Gutman, G., Gulev, S., Qi, J., Prishchepov, A., 2017. Northern Eurasia Future Initiative (NEFI): facing the challenges and pathways of global change in the twenty-first century. Prog. Earth Planet. Sci. 4 (1), 41.

Gu, H., Wang, G., Yu, Z., Mei, R., 2015. Assessing CMIP5 general circulation model simulations of precipitation and temperature over China. Int. J. Climatol. 35 (9), 2431–2440.

Gudmundsson, L., 2016. qmap: Statistical transformations for post-processing climate model output (R package). R package version 1.0-4. CRAN. Available at: ⟨https://cran.r-project.org/package=qmap⟩ (Accessed: 11 October 2024).

Guo, E., Zhang, J., Wang, Y., Quan, L., Zhang, R., 2017. Assessing spatiotemporal variation of drought and its impact on maize yield in Northeast China. J. Hydrol. 553, 231–247.

Hanway, J., 1966. How a corn plant develops. Iowa Agricultural Experiment Station Special Report No. 48. Iowa State University, Ames, IA. ⟨https://publications.iowa.gov/18027/1/How%20a%20corn%20plant%20develops001.pdf⟩.

Harvey, C.A., Saborio-Rodríguez, M., Martinez-Rodríguez, M.R., Viguera, B., Chain-Guadarrama, A., Vignola, R., Alpizar, F., 2018. Climate change impacts and adaptation among smallholder farmers in Central America. Agric. Food Secur. 7 (1), 57.

Hatfield, J.L., Prueger, J.H., 2015. Temperature extremes: effect on plant growth and development. Weather Clim. Extrem. 10, 4–10.

Hatfield, J.L., Boote, K.J., Kimball, B.A., Ziska, L.H., Izaurralde, R.C., Ort, D., Thomson, A.M., Wolfe, D., 2011. Climate impacts on agriculture: implications for crop production. Agron. J. 103 (2), 351–370.

Heng, L.K., Hsiao, T., Evett, S., Howell, T., Steduto, P., 2009. Validating the FAO AquaCrop model for irrigated and water-deficient field maize. Agron. J. 101 (3), 488–498.

Herrero, M.P., Johnson, R.R., 1980. High temperature stress and pollen viability of maize. Crop Sci. 20 (6), 796–800.

Hock, R., Rasul, G., Adler, C., Cáceres, B., Gruber, S., Hirabayashi, Y., Jackson, M., Kääb, A., Kang, S., Kutuzov, S., Milner, A., Molau, U., Morin, S., Orlove, B., Steltzer, H., 2019. High Mountain Areas. In: Pörtner, H.-O., Roberts, D.C., Masson-Delmotte, V., Zhai, P., Tignor, M., Poloczanska, E., Mintenbeck, K., Alegría, A., Nicolai, M., Okem, A., Petzold, J., Rama, B., Weyer, N.M. (Eds.), IPCC Special Report on the Ocean and Cryosphere in a Changing Climate. Cambridge University Press, Cambridge, UK and New York, NY, USA, pp. 131–202. https://doi.org/10.1017/9781009157964.004.

Hsiao, T.C., Heng, L., Steduto, P., Rojas-Lara, B., Raes, D., Fereres, E., 2009. AquaCrop — the FAO crop model to simulate yield response to water: III. Parameterization and testing for maize. Agron. J. 101 (3), 448–459.

Huang, A., Zhou, Y., Zhang, Y., Huang, D., Zhao, Y., Wu, H., 2014. Changes of the annual precipitation over central Asia in the twenty-first century projected by multimodels of CMIP5. J. Clim. 27 (17), 6627–6646.

Jägermeyr, J., Müller, C., Ruane, A.C., Elliott, J., Balkovic, J., Castillo, O., Faye, B., Foster, I., Folberth, C., Franke, J.A., Fuchs, K., 2021. Climate impacts on global agriculture emerge earlier in new generation of climate and crop models. Nat. Food 2 (11), 873–885.

Jain, S., Salunke, P., Mishra, S.K., Sahany, S., 2019. Advantage of NEX-GDDP over CMIP5 and CORDEX data: Indian summer monsoon. Atmos. Res. 228, 152–160.

Jiang, J., Zhou, T., Chen, X., Zhang, L., 2020. Future changes in precipitation over Central Asia based on CMIP6 projections. Environ. Res. Lett. 15 (5), 054009.

Jiang, R., He, W., He, L., Yang, J.Y., Qian, B., Zhou, W., Liu, J., 2021. Modelling adaptation strategies to reduce adverse impacts of climate change on maize cropping system in northeast China. Sci. Rep. 11 (1), 810.

Kamphake, L.J., Hannah, S.A., Cohen, J.M., 1967. Automated analysis for nitrate by hydrazine reduction. Water Res. 1 (3), 205–216.

Kapitsa, V., Shahgedanova, M., Machguth, H., Severskiy, I., Medeu, A., 2020. Assessment of changes in mass balance of the Tuyuksu group of glaciers, northern Tien Shan between 1958 and 2016 using ground-based observations and Pleiades satellite imagery. Front. Earth Sci. 8, 259.

Kato, E., Nkonya, E., Koo, J., Bobojonov, I., 2012. Climate change effects on cotton and potato and adaptation options in Central Asia: evidence from DSSAT crop simulation model. Project Report. IFPRI, Washington, USA. ⟨https://core.ac.uk/download/389280244.pdf⟩ (Available at).

Keulen, H. van, 2013. Simulation models as tools for crop management. Sustainable Food Production. Springer, New York, NY, pp. 1459–1476.

Kimball, B.A., 2016. Crop responses to elevated CO_2 and interactions with H_2O, N, and temperature. Curr. Opin. Plant Biol. 31, 36–43.

Kokarev, A., Smirnov, A., Medeu, A., Blagoveshchenskiy, V., Gabbasov, J., Kenzhebaev, R., 2023. Results of geodetic measurements of the mass balance of some glaciers in the Trans-Ili Alatau. Water Resour. 50, S24–S32.

Konzmann, M., Gerten, D., Heinke, J., 2013. Climate impacts on global irrigation requirements under 19 GCMs, simulated with a vegetation and hydrology model. Hydrol. Sci. J. 58 (1), 88–105.

Lazarov, R., 1965. Coefficients for determination of leaf area in some crops. Plant Sci. 2 (2), 27–37.

Lin, W.Q., Chen, H.P., 2020. Assessment of model performance of precipitation extremes over the mid-high latitude areas of Northern Hemisphere: from CMIP5 to CMIP6. Atmos. Ocean. Sci. Lett. 13 (6), 598–603.

Lin, Y., Liu, Z., Liu, J., Wang, S., Huang, W., 2017. Potential impacts of climate change and adaptation on maize in northeast China. Agron. J. 109 (4), 1476–1490.
Lioubimtseva, E., Henebry, G.M., 2009. Climate and environmental change in arid Central Asia: impacts, vulnerability, and adaptations. J. Arid Environ. 73 (11), 963–977.
Liu, B., Liu, L., Tian, L., Cao, W., Zhu, Y., Asseng, S., 2014. Post-heading heat stress and yield impact in winter wheat of China. Glob. Change Biol. 20 (2), 372–381.
Liu, B., Asseng, S., Müller, C., et al., 2016. Similar estimates of temperature impacts on global wheat yield by three independent methods. Nat. Clim. Change 6 (12), 1130–1136.
Liu, Z., Yang, X., Hubbard, K.G., Lin, X., 2013. Negative effects of climate warming on maize yield are reversed by changing sowing date and cultivar selection in Northeast China. Glob. Change Biol. 19 (11), 3481–3492.
Loague, K., Green, R.E., 1991. Statistical and graphical methods for evaluating solute transport models: overview and application. J. Contam. Hydrol. 7 (1–2), 51–73.
Lobell, D.B., Schlenker, W., Costa-Roberts, J., 2011. Climate trends and global crop production since 1980. Science 333 (6042), 616–620.
Lobell, D.B., Roberts, M.J., Schlenker, W., Braun, N., Little, B.B., Rejesus, R.M., Hammer, G.L., 2014. Greater sensitivity to drought accompanies maize yield increase in the U. S. Midwest Sci. 344 (6183), 516–519.
Mamadiyarov, B.S., Bazarbayev, A.T., Zuga, K., Bayekenova, M.K., Kalybekova, Y.M., 2015. Research on Water Quality of the Transboundry Ili River and Its Tributaries. Biosci. Biotechnol. Res. Asia 12 (1), 119–132.
Mbow, C., Rosenzweig, C., Barioni, L.G., Benton, T.G., Herrero, M., Krishnapillai, M., Liwenga, E., Pradhan, P., Rivera-Ferre, M.G., Sapkota, T., Tubiello, F.N., Xu, Y., 2019. Food Security. In: Shukla, P.R., Skea, J., Calvo Buendia, E., Masson-Delmotte, V., Pörtner, H.-O., Roberts, D.C., Zhai, P., Slade, R., Connors, S., van Diemen, R., Ferrat, M., Haughey, E., Luz, S., Neogi, S., Pathak, M., Petzold, J., Portugal Pereira, J., Vyas, P., Huntley, E., Kissick, K., Belkacemi, M., Malley, J. (Eds.), Climate Change and Land: an IPCC special report on climate change, desertification, land degradation, sustainable land management, food security, and greenhouse gas fluxes in terrestrial ecosystems. Cambridge University Press, Cambridge, UK and New York, NY, USA, pp. 437–550.
Mirzabaev, A., 2013. Impacts of weather variability and climate change on agricultural revenues in Central Asia. Q. J. Int. Agric. 52 (3), 237–252.
Morgounov, A., Abugalieva, A., Martynov, S., 2014. Effect of climate change and variety on long-term variation of grain yield and quality in winter wheat in Kazakhstan. Cereal Res. Commun. 42 (1), 163–172.
Murzakulova, A., Schmidt-Vogt, D., Balla, D., Darr, D., Hamidov, A., Kasymov, U., Mendelevitch, R., Orazgaliyev, S., 2019. Water for agriculture and other economic sectors. In: Xenarious., S., Schmidt-Vogt, D., Qadir, M., Janusz-Pawletta, B., Abdullaev, I. (Eds.), The Aral Sea Basin. Routledge, London, pp. 86–99.
Nizamov, S., Riskieva, K., Umarov, M., Kuziev, J., Mirsodikov, M., 2023. Effect of cadmium on agrochemical and ecological status of irrigated soils. In: E3S Web of Conferences, 389. EDP Sciences, p. 03038.
Pavlova, V.N., Varcheva, S.E., Bokusheva, R., Calanca, P., 2014. Modelling the effects of climate variability on spring wheat productivity in the steppe zone of Russia and Kazakhstan. Ecol. Model. 277, 57–67.
Peng, Y., Li, X., Li, C., 2012. Temporal and spatial profiling of root growth revealed novel response of maize roots under various nitrogen supplies in the field. PLoS ONE 7 (5), e37726.
Pieczonka, T., Bolch, T., 2015. Region-wide glacier mass budgets and area changes for the Central Tien Shan between ~1975 and 1999 using Hexagon KH-9 imagery. Glob. Planet. Change 128, 1–13.
Poggio, L., De Sousa, L.M., Batjes, N.H., Heuvelink, G.B., Kempen, B., Ribeiro, E., Rossiter, D., 2021. SoilGrids 2.0: producing soil information for the globe with quantified spatial uncertainty. Soil 7 (1), 217–240.
Raes, D., Steduto, P., Hsiao, T.C., Fereres, E., 2009. AquaCrop — the FAO crop model to simulate yield response to water: II. Main algorithms and software description. Agron. J. 101 (3), 438–447.
Ragab, R., 2002. A holistic generic integrated approach for irrigation, crop and field management: the SALTMED model. Environ. Model. Softw. 17 (4), 345–371.
Ragab, R., 2015. Integrated management tool for water, crop, soil and N-fertilisers: the SaltMed model. Irrig. Drain. 64 (1), 1–12.
Ray, D.K., Gerber, J.S., MacDonald, G.K., West, P.C., 2015. Climate variation explains a third of global crop yield variability. Nat. Commun. 6, 5989.
Ray, D.K., West, P.C., Clark, M., Gerber, J.S., Prishchepov, A.V., Chatterjee, S., 2019. Climate change has likely already affected global food production. PLoS ONE 14 (5), e0217148.
Reiter, P., Andersen, L., Weidinger, T., Haimberger, L., 2016. Bias correction of ENSEMBLES precipitation data with focus on the effect of the length of the calibration period. Meteorol. Z. 25 (1), 85–96.
Reyer, C.P.O., Otto, I.M., Adams, S., Albrecht, T., Baarsch, F., Cartsburg, M., Coumou, D., Eden, A., Ludi, E., Marcus, R., Mengel, M., 2017. Climate change impacts in Central Asia and their implications for development. Reg. Environ. Change 17 (6), 1639–1650.
Rosenzweig, C., Jones, J.W., Hatfield, J.L., Ruane, A.C., Boote, K.J., Thorburn, P., Antle, J.M., Nelson, G.C., Porter, C., Janssen, S., Asseng, S., 2013. The Agricultural Model Intercomparison and Improvement Project (AgMIP): protocols and pilot studies. Agric. For. Meteorol. 170, 166–182.
Rosenzweig, C., Elliott, J., Deryng, D., Ruane, A.C., Müller, C., Arneth, A., Boote, K.J., Folberth, C., Glotter, M., Khabarov, N., Neumann, K., 2014. Assessing agricultural risks of climate change in the 21st century in a global gridded crop model intercomparison. In: Proceedings of the National Academy of Sciences, 111, pp. 3268–3273.
Ryzak, M., Bieganowski, A., 2011. Methodological aspects of determining soil particle-size distribution using the laser diffraction method. J. Plant Nutr. Soil Sci. 174 (4), 624–633.
Sacks, W.J., Cook, B.I., Buenning, N., Levis, S., Helkowski, J.H., 2009. Effects of global irrigation on the near-surface climate. Clim. Dyn. 33 (2), 159–175.
Saddique, Q., Liu, D., Wang, B., Feng, P., He, J., Ajaz, A., Ji, J., Xu, J., 2020. Analyzing adaptation strategies for maize production under future climate change in Guanzhong Plain, China. Mitig. Adapt. Strateg. Glob. Change 25 (8), 1523–1543.
Saidaliyeva, Z., Shahgedanova, M., Yapiyev, V., Wade, A.J., Akbarov, F., Esenaman uulu, M., Kalashnikova, O., Kapitsa, V., Kasatkin, N., Rakhimov, I., Satylkanov, R., Sayakbaev, D., Semakova, E., Severskiy, I., Petrov, M., Umirzakov, G., Usubaliev, R., 2024. Precipitation in the mountains of Central Asia: isotopic composition and source regions. Atmos. Chem. Phys. 24, 12203–12224.
Schmitz, A., Meyers, W.H. (Eds.), 2015. Transition to Agricultural Market Economies: The Future of Kazakhstan, Russia and Ukraine, 258. CABI, Wallingford, UK.
Sha, Y., Zheng, L., Zhanhong, H., Huang, Y., Shao, H., Feng, G., Chen, F., Mi, G., 2024. Root growth, root senescence and root system architecture in maize under conservative strip tillage system. Plant Soil 495, 253–269.
Shahgedanova, M., Afzal, M., Severskiy, I., Usmanova, Z., Saidaliyeva, Z., Kapitsa, V., 2018. Changes in the mountain river discharge in the Northern Tien Shan since the mid-20th century: analysis of a homogeneous daily streamflow dataset from seven catchments. J. Hydrol. 564, 1133–1152.
Shahgedanova, M., Kapitsa, V., Machguth, H., Severskiy, I., Medeu, A., 2020. Emptying water towers? Impacts of future climate and glacier change on river discharge in the Northern Tien Shan, Central Asia. Water 12 (3), 627.
Shamrikova, E.V., Vanchikova, E.V., Lu-Lyan-Min, E.I., Kubik, O.S., Zhangurov, E.V., 2023. Which method to choose for measurement of oranic and inorganic carbon content in carbonate-rich soils? Advantages and disadvantages of dry and wet chemistry. CATENA 228, 107151.
Shannon, S., Smith, R., Wiltshire, A., Payne, T., Huss, M., Betts, R., Caesar, J., Koutroulis, A., Jones, D., Harrison, S., 2019. Global glacier volume projections under high-end climate change scenarios. Cryosphere 13 (4), 325–350.
Sherzod, N., Djumaniyazova, Y., Khamzina, A., Khasanov, F., Li, Y., Feng, A., 2023. Applicability of the AquaCrop model for simulating winter wheat under a semi-arid climate in Uzbekistan. J. Arid Land Stud. 33 (2), 91–104.
Sokolov, S.I., Assing, I.A., Kurmangaliyev, A.B., Serpikov, S.K., 2017. Pochvy Kazakhstana. Vypusk 4: Pochvy Almaatinskoj Oblasti (Soils of Kazakhstan, Part 4: Soils of the Almaty Region). KazBookTrade Publishers, Almaty, p. 472 (In Russian).
Sommer, R., Glazirina, M., Yuldashev, T., Otarov, A., Ibraeva, M., Martynova, L., Bekenov, M., Kholov, B., Ibragimov, N., Kobilov, R., Karaev, S., 2013. Impact of climate change on wheat productivity in Central Asia. Agric. Ecosyst. Environ. 178, 78–99.
Song, X., Song, S., Sun, W., Mu, X., Wang, S., Li, J., Li, Y., 2019. Past and future changes in regional crop water requirements in northwest China. Theor. Appl. Climatol. 137 (3-4), 2203–2215.
Steduto, P., Hsiao, T.C., Raes, D., Fereres, E., 2009. AquaCrop — the FAO crop model to simulate yield response to water: I. Concepts and underlying principles. Agron. J. 101 (3), 426–437.
Stocker, B.D., Wang, H., Smith, N.G., Harrison, S.P., Keenan, T.F., Sandoval, D., Davis, T., Prentice, I.C., 2020. P-model v1.0: an optimality-based light use efficiency model for simulating ecosystem gross primary production. Geosci. Model Dev. 13 (3), 1545–1581.
Tao, F., Zhang, Z., 2010. Adaptation of maize production to climate change in North China Plain: quantify the relative contributions of adaptation options. Eur. J. Agron. 33 (2), 103–116.
Taylor, K.E., 2001. Summarizing multiple aspects of model performance in a single diagram. J. Geophys. Res. Atmospheres 106 (D7), 7183–7192.
Tegegne, D., Schmitter, P., Worqlul, A.W., Lefore, N., 2025. Estimating crop coefficients for vegetable production and agricultural water management under climate change in sub-humid tropics. Front. Water 7, 1355154.
Teutschbein, C., Seibert, J., 2012. Bias correction of regional climate model simulations for hydrological climate-change impact studies: review and evaluation of different methods. J. Hydrol. 12–29, 456–457.
Thevs, N., Nurtazin, S., Beckmann, V., Salmyrzauli, R., Khalil, A., 2017. Water consumption of agriculture and natural ecosystems along the Ili River in China and Kazakhstan. Water 9 (3), 207.
Thrasher, B., Maurer, E.P., McKellar, C., Duffy, P.B., 2012. Bias correcting climate model simulated daily temperature extremes with quantile mapping. Hydrol. Earth Syst. Sci. 16 (9), 3309–3314.
Timlin, D., Paff, K., Han, E., 2024. The role of crop simulation modeling in assessing potential climate change impacts. Agrosystems Geosci. Environ. 7 (1), e20453.
Ummenhofer, C.C., Xu, H., Twine, T.E., Girvetz, E.H., McCarthy, H.R., Chhetri, N., Nicholas, K.A., 2015. How climate change affects extremes in maize and wheat yield in two cropping regions. J. Clim. 28 (12), 4653–4687.
Vakulchuk, R., Daloz, A.S., Overland, I., Sagbakken, H.F., Standal, K., 2022. A void in Central Asia research: climate change. Cent. Asian Surv. 42 (1), 1–20.
Van Genuchten, M.T., 1980. A closed-form equation for predicting the hydraulic conductivity of unsaturated soils. Soil Sci. Soc. Am. J. 44 (5), 892–898.
Viviroli, D., Weingartner, R., 2004. The hydrological significance of mountains: from regional to global scale. Hydrol. Earth Syst. Sci. 8 (6), 1017–1030.
Wade, A.J., Yapiyev, V., Shahgedanova, M., Saidaliyeva, Z., Madibekov, A., Severskiy, I., 2024. Cryosphere and land cover influence on stream water quality in Central Asia's glacierized catchments. Sci. Total Environ. 939, 173525.
Watanabe, M., Suzuki, T., O'ishi, R., Komuro, Y., Watanabe, S., Emori, S., Takemura, T., Chikira, M., Ogura, T., Sekiguchi, M., Takata, K., 2010. Improved climate simulation

by MIROC5: mean states, variability, and climate sensitivity. J. Clim. 23 (23), 6312–6335.
Wolf, D.D., Carson, E.W., Brown, R.H., 1972. Leaf area index and specific leaf area determinations. J. Agron. Educ. 1 (1), 24–27.
Wu, L., Wang, S., Bai, X., Luo, W., Tian, Y., Zeng, C., Luo, G., He, S., 2021. Impacts of climate change on vegetation phenology and net primary productivity in arid Central Asia. Sci. Total Environ. 796, 149055.
Wu, T., Yu, R., Zhang, F., Wang, Z., Dong, M., Wang, L., Jin, X., Chen, D., Li, L., 2014. An overview of BCC climate system model development and application for climate change studies. J. Meteorol. Res. 28 (1), 34–56.
Yang, C., Fraga, H., Van Ieperen, W., Santos, J.A., 2017. Assessment of irrigated maize yield response to climate change scenarios in Portugal. Agric. Water Manag. 184, 178–190.
Yao, J., Chen, Y., Yu, X., Zhao, Y., Guan, X., Yang, L., 2022. Recent climate and hydrological changes in a mountain–basin system in Xinjiang, China. Earth-Sci. Rev. 226, 103957.
Yapiyev, V., Sagintayev, Z., Verhoef, A., Kassymbekova, A., 2017. Essentials of endorheic basins and lakes: a review in the context of current and future water resource management and mitigation activities in Central Asia. Water 9 (10), 798.
Yapiyev, V., Wade, A.J., Shahgedanova, M., Saidaliyeva, Z., Madibekov, A., Severskiy, I., 2021. The hydrochemistry and water quality of glacierized catchments in Central Asia: a review of the current status and anticipated change. J. Hydrol. Reg. Stud. 38, 100960.
Yu, X., Zhao, Y., Ma, X., Yao, J., Li, H., 2018. Projected changes in the annual cycle of precipitation over Central Asia by CMIP5 models. Int. J. Climatol. 38 (15), 5589–5604.
Zheng, H., Bian, Q., Yin, Y., Ying, H., Yang, Q., Cui, Z., 2018. Closing water productivity gaps to achieve food and water security for a global maize supply. Sci. Rep. 8, 14762.
Zomer, R.J., Xu, J., Trabucco, A., 2022. Version 3 of the global aridity index and potential evapotranspiration database. Sci. Data 9, 409.